KLOE Memo 345
June 2008

Study of the $e^+e^- \to \omega\pi^0 \to \pi^+\pi^-\pi^0\pi^0$ process using KLOE data

A. De Santis [a], S. Giovannella [b],

[a] *Dipartimento di Fisica dell'Università "Sapienza" e Sezione INFN, Roma, Italy.*

[b] *Laboratori Nazionali di Frascati dell'INFN, Frascati, Italy.*

Abstract

We report the measurement of the visible cross section for the $e^+e^-\to\omega\pi^0$ in the $\pi^+\pi^-\pi^0\pi^0$ final state performed using 450 pb^{-1} of integrated luminosity collected in the 2001-2002 data-taking period plus $\sim$150 pb^{-1} of data collected *off-peak* at the end of KLOE data-taking. The dependence of the cross sections on the center of mass energy, $\sqrt{s}$, has been studied in the range from 1000 to 1030 MeV . In this range of $\sqrt{s}$ the interference between this continuum process and the resonant process $\phi\to\omega\pi^0$ has been observed and the relative amplitude has been measured. This measurement allows to determine the amplitude for the OZI and G-parity suppressed decay $\phi\to\omega\pi^0$: $BR(\phi \to \omega\pi^0) = (4.4 \pm 0.6) \times 10^{-5}$.

Moreover using the reference value of the cross section at m_ϕ for the $e^+e^- \to \omega\pi^0\to \pi^+\pi^-\pi^0\pi^0$ process together with the corresponding measurement for the $\omega\pi^0\to\pi^0\pi^0\gamma$ we are able to obtain a precise determination of the principal ω decay widths: $\Gamma(\omega \to \pi^0\gamma)/\Gamma(\omega \to \pi^+\pi^-\pi^0) = 0.0897 \pm 0.0016$. Combining this value with the measurements of rarest ω BR's we get the most precise value for the dominant ω's BR: $BR(\omega \to \pi^+\pi^-\pi^0) = (90.24 \pm 0.19)\%$ and $BR(\omega \to \pi^0\gamma) = (8.09 \pm 0.14)\%$.

Contents

1 Introduction

Due to the large statistics collected by KLOE around the ϕ resonance, the study of ϕ rare decays having branching ratios of 10^{-4}-10^{-5} becomes possible. One such decay is the OZI and G-parity violating $\phi \to \omega\pi^0$ process. To study this reaction we have to observe the cross section of $e^+e^- \to \omega\pi^0$ in the center of mass (CoM) energy around the ϕ meson resonance. From the parameter describing this cross section is possible to determine the amplitude of the ϕ decay. The amplitude for such a process can be represented in a VMD description [1] as the sum of two different amplitudes [1] as show in Fig. 1.

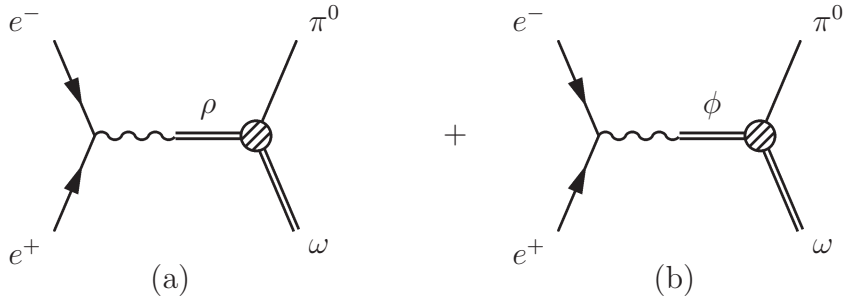

Fig. 1. Amplitude for $e^+e^- \to \omega\pi^0$. Non resonant (a) and resonant (b) term.

The Born cross section, taking into account the interference, could be expressed in the form:

$$\sigma(E) = \sigma_{nr}(E) \left| 1 - Z \frac{m_\phi \Gamma_\phi}{D_\phi} \right|^2 \tag{1}$$

where $\sigma_{nr}(E)$ is the cross section for the non resonant process, Z is a complex parameter that is equal to the ratio of the two decay amplitudes, m_ϕ,Γ_ϕ and D_ϕ are mass, width and inverse propagator of the ϕ-meson respectively. Since the parameter Z has this kind of interpretation is possible to define:

$$BR(\phi \to \omega\pi^0) = \frac{\sigma_{nr}(m_\phi)|Z|^2}{\sigma_\phi}$$

[1] This approximation depends on the final state considered. In the case of $\pi^+\pi^-\pi^0\pi^0$ final state the assumption is valid, while in the case of $\pi^0\pi^0\gamma$ final state is necessary to consider also other VMD diagrams that can interfere.

2 MC generator

The simplest way to simulate the process $e^+e^- \to \omega\pi^0 \to \omega\pi^0$ is a chain of two decays, $e^+e^- \to \omega\pi^0$ followed by $\omega \to \pi^-\pi^+\pi^0$ without dynamics. In the first decay the ω mass is extracted according to a Breit-Wigner distribution shaped with ω mass and width, with polar angular distribution simulated according to $d\sigma/d\Omega = 1 + \cos^2\vartheta$ (standard for Vector-Pseudoscalar (VP) production). Without assumption on the dynamics, the secondary decay can be simulated as a pure phase space decay, i.e. a flat density distribution in the Dalitz-plot.

This description of the process did not include two dynamical features that are expected, and observed, in a decay of a vector meson into three pseudo-scalars:

- the density distribution, in the plane defined by T^0 (kinetic energy of the π^0) and $\Delta T^\pm$ (difference between kinetic energy of the charged pions) $\mathcal{D}(\Delta T^\pm, T^0)$ has to be proportional to $|\overrightarrow{p}_{\pi^+} \times \overrightarrow{p}_{\pi^-}|^2$;
- in the ω rest frame (RF_ω), the angle between the normal to the pions' decay plane and the flight direction of the ω has to be distributed according to $dN/d\vartheta_n = \sin^2\vartheta_n$.

The data distribution, shown in Fig. 2, confirms this expectation.

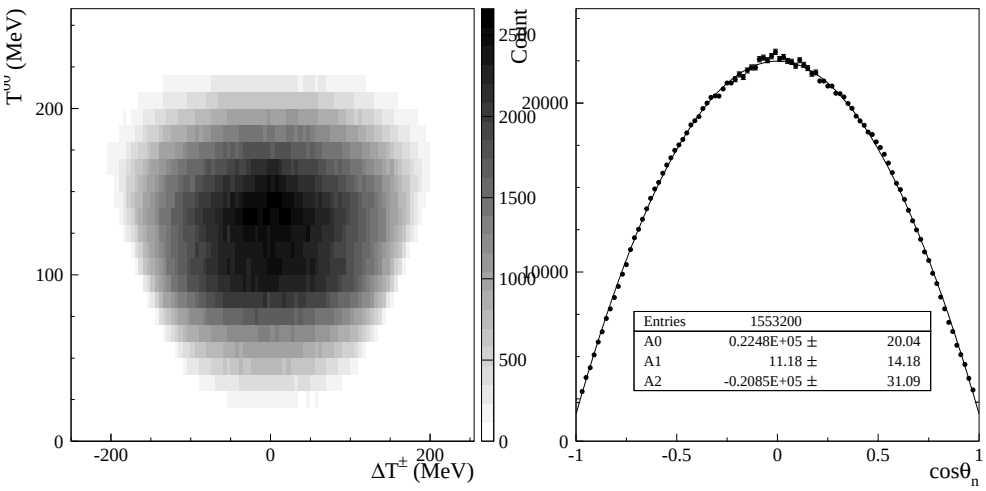

Fig. 2. Data distribution. Left: density distribution in the plane $\Delta T^\pm$, T^0. The non uniform distribution is clearly visible. Right: angular distribution of the normal to decay plane in RF_ω (see text). Black dots are data while the black line is the fit with a second order polynomial. The linear coefficient is compatible with zero and the other two have opposite sign as for the hypothesis $dN/d\vartheta_n \propto \sin^2\vartheta_n \Rightarrow dN/d\cos\vartheta_n \propto 1 - \cos^2\vartheta_n$.

In order to introduce these dynamical features in the Monte Carlo simulation

we have developed a dedicated generator [2] for this process based on Vector Meson Dominance (VMD) description according to [2], where six different diagrams contribute (see Fig. 3). Comparison between data distributions (Fig. 2) with the MC distributions, shown in Fig. 4, demonstrates immediately the improvements in the description of data by our generator.

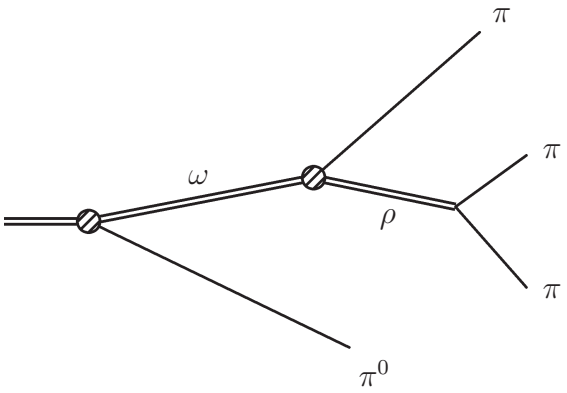

Fig. 3. General VMD diagram for $\pi^+\pi^-\pi^0\pi^0$. The complete matrix element is the modulus squared of the sum over all possible values of the ρ meson charge and the π^0's permutation for a total of six different diagrams. The circle in the vertex between vector mesons represents the form factor in the coupling. In our generator we use a simple dipolar expression $F_\omega(Q^2) = \frac{1+M_\omega^2/\Lambda^2}{1+Q^2/\Lambda^2}$ were Λ stands for the energy scale for the process ($\Lambda = 1$ GeV). In the propagator of ρ meson we have introduced an energy dependent description of the width: $\Gamma_\rho = \Gamma_0 \times \frac{g(q^2)}{g(M_\rho)}$ with $g(s) = s^{-1/2}(s - (\sum_f m_f)^2)^{3/2}$.

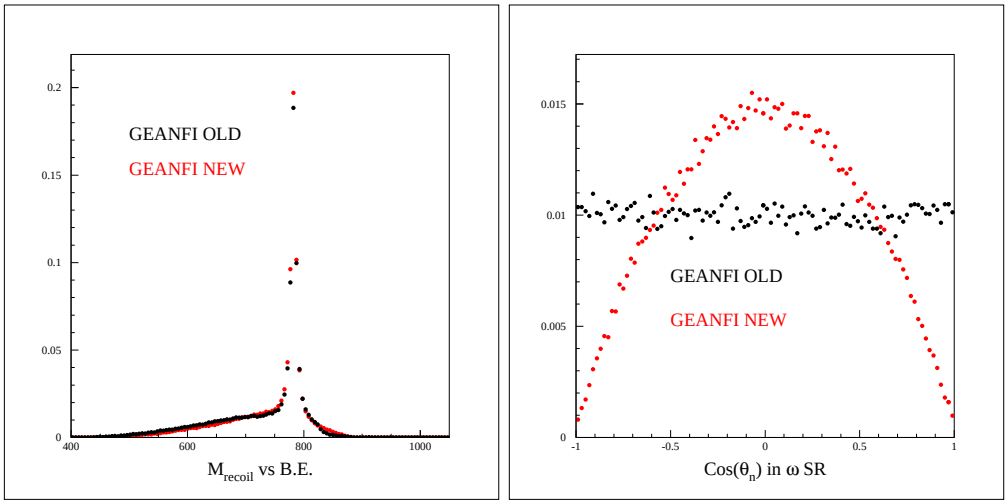

Fig. 4. MC comparison. Bottom left: π^0 recoil mass ($|P_{Tot} - P_{\pi^0}|$). Bottom right: angular distribution of the normal to decay plane in RF_ω. The difference induced by the dynamical features in the angular distributions are clearly visible.

[2] A more detailed description is available in appendix § A

3 Data and Monte Carlo samples

In this analysis, the whole available statistics collected in 2001-2002 data taking period, corresponding to 450 pb^{-1}, has been used. In order to expand the analysis in a wider energy range far from ϕ, we have also analysed the data collected between the end of 2005 and the begin of 2006, referred as *off-peak* data (RUN # 41900 - 43000). The data analysis is done using the charged radiative DST (DRC) selected by the Event Classification (ECL) algorithm [3]. The DST are produced with datarec version 13 and 14 for the 2001-2002 data and version 24-26 for the off-peak [4].

For each run ($L_{int} \simeq 200$ nb^{-1}) the large angle Bhabha (vlabha) events are used to estimate both the luminosity and the beam parameter (beam position, ϕ boost, $\sqrt{s}$, ...). Since we study the dataset as function of center of mass energy, the luminosity for each run has been evaluated from the vlabha [3] normalized with the corresponding value for the cross section obtained from *BABAYAGA 3.0* [4] [5,6].

In order to classify our sample the most important parameter is the center of mass energy, shown in Fig. 5 as a function of the run number. Since we know $\sqrt{s}$ with a precision of 30 keV, we have divided all events in bins of 100 keV. Only bins with an integrated luminosity of at least 1 pb^{-1} have been considered in the present analysis. For the *off-peak* events these bins have been grouped to increase statistics. The absolute calibration of the KLOE center of mass energy has been performed fitting the ϕ-scan data to extract the ϕ mass [7]. Comparing result with the ϕ mass obtained by SND with the depolarization method we obtain a global energy shift of 150 keV. This correction has been applied when analysing our sample.

For Monte Carlo (MC) samples, we have used the MRC DSTs of the official KLOE 2001/2002 MC production for the background (*all_phys* card) in the charged radiative stream, whose integrated luminosity is 1/5 with respect to

[3] The number of very large angle bhabha events has been obtained for the run number $RUN with a query to the database: `dbonl "select run_nr,version,sum(vlabha) from logger.datarec_runs group by run_nr,version having run_nr=$RUN and version = (select version from logger.datarec_maxver where run_nr=$RUN and stream_id=4 and run_nr=$RUN)"` for the *off-peak* data and `‘dbonl "select run_nr,version,sum(vlabha) from logger.datarec_runs group by run_nr,version having run_nr=$RUN and version = ( select max(version) from logger.datarec_data where stream_id=4 and run_nr=$RUN and version < 18 )"`

[4] The used cross section is: $\sigma_{vlabha} = (1335. - 0.8475 \times \sqrt{s}) * \rho_{KLOE}$, where $\rho_{KLOE} = 0.9104$ is a correction factor that takes into account detection efficiency.

real data. This MC production has been reconstructed whit datarec version 18. For the *off-peak* data we have used the relative MC production (*all_phys* card with luminosity scale factor 2) in which our generator is already included. Since this last production has wrong normalization with respect to the real data [5] we also have used the production done with *omegapi* card in which only the ω's decays are simulated. Both have been reconstructed with datarec version 26.

For the signal MC simulation relative to 2001/2002 data we have used a dedicated production. This simulation, as the official MC, is done on a run by run basis including: beam parameters variations, background conditions and detector response. The luminosity scale factor is 5 and the datarec version used is the 26.

In order to simulate the continuum background $e^+e^- \to a_1\pi \to \pi^+\pi^-\pi^0\pi^0$ we have also produced a dedicated MC sample using a customized version of GEANFI. Similarly to the signal simulation, also in this case the MC production has been done for the entire run range on a run by run basis.

4 Signal and backgrounds

In this work we study the intermediate state $\omega\pi^0$ through the final state $\pi^+\pi^-\pi^0\pi^0$, having two charged tracks and four photons in the final state.

The background sources can be divided in two main categories: ϕ backgrounds and continuum backgrounds. The ϕ backgrounds is due to the following process:

(1) $\phi \to K_S K_L$, with $K_S \to 2\pi^0$ *and* $K_L \to K_{e3}(K_{\mu 3})$ with a relative fractions of 42(39)%, and $K_L \to \pi\pi$ (CP) with a fraction of 11%.
(2) $\phi \to K^+K^-$, with $K2_\pm \to \pi^\pm\pi^0$
(3) $\phi \to \eta\gamma$, with $\eta \to \pi^-\pi^+\pi^0$
(4) $\phi \to \rho\pi \to \pi^-\pi^+\pi^0$

The first two have the same final state of the signal, while the last two produce two tracks and four clusters because of machine background and/or cluster splitting.

The continuum process that contribute to the background is the $a_1\pi \to \pi^+\pi^-\pi^0\pi^0$. The $a_1\pi$ production has been studied with high accuracy in the

[5] The relative normalization between ϕ cross section and continuum process has been calculated only in the range 1010-1030 MeV. This implies that for the *off-peak* events the relative fraction of $\omega\pi^0$ events is much less than one could expect.

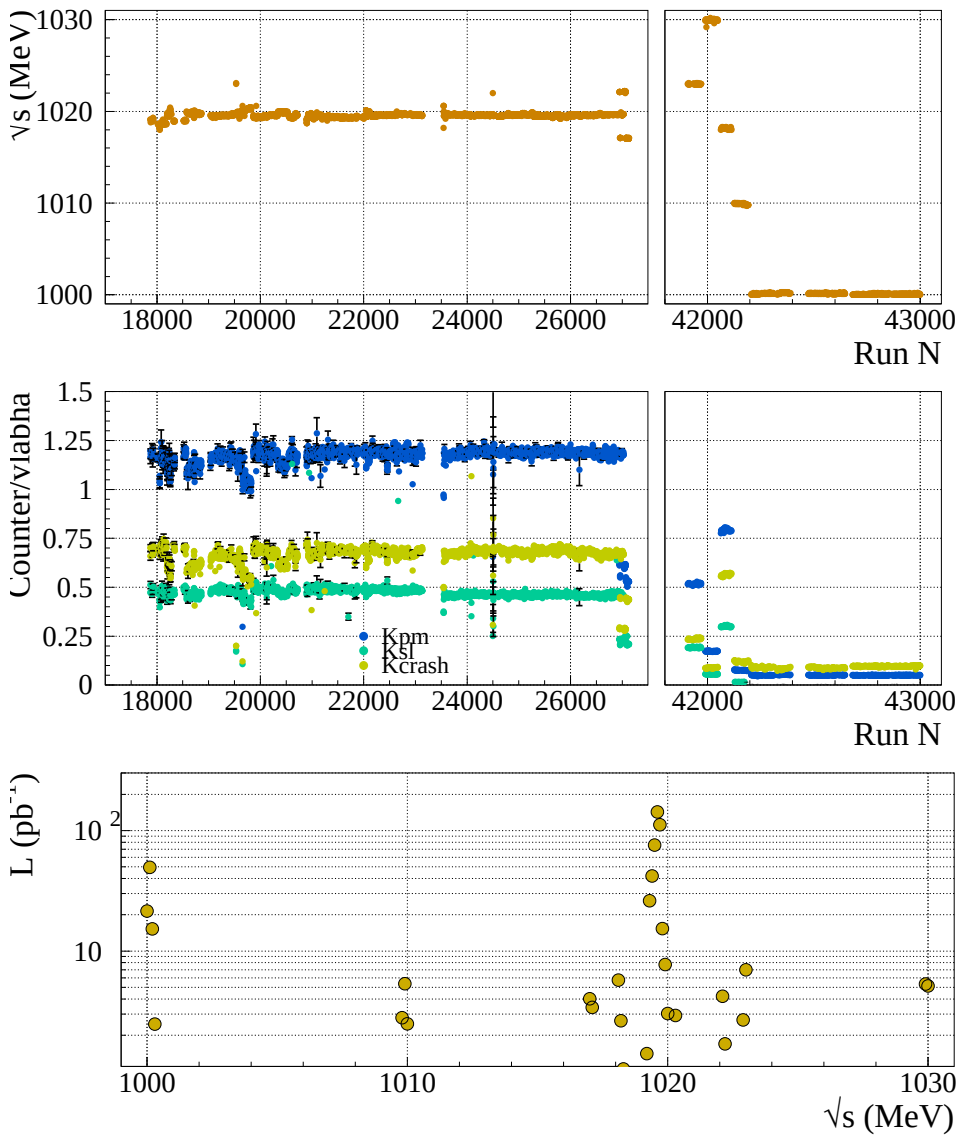

Fig. 5. Top: center of mass energy as a function of the run number. The $\sqrt{s}$value in the left panel is for 2001-2002 data , while in the right panel for the *off-peak* data, where the large spread in CoM energy is shown. Center: Event counter normalized to the run luminosity as a function of run number. On the left panel counters for 2001-2002, while on the right for the *off-peak*. The observed behavior for the counter is strictly correlated to value of the energy. Bottom: integrated luminosity as a function of center of mass energy.

final state $\pi^+\pi^-\pi^+\pi^-$ [8]. Assuming the $a_1\pi$ dominance [2] we expect a cross section between $0.2 \div 0.4$ nb.

In order to study the background components some useful variables are defined:

M_{recoil} **:** the recoil mass with respect to a reconstructed π^0. This is defined

as the difference between total four-momentum and the four-momentum of the π^0 ($|P_{Tot} - P_{\pi^0}|$). Since we have two π^0's per event, we have two values of this variable.

$M_{\pm}$ **:** the invariant mass of the charged track pair in the pion hypothesis ($|P_{\pi^+} + P_{\pi^-}|$).

M_{mix} **:** the invariant mass of the pion pair, obtained using a charged and a neutral π. Since there are two charged tracks and two reconstructed π^0 in the event, four values for this variable are obtained.

In Fig. 6, distributions M_{recoil}, $M_{\pm}$ and M_{mix} obtained from MC are shown. In each of them, a characteristic peak due to one of the backgrounds channels is present.

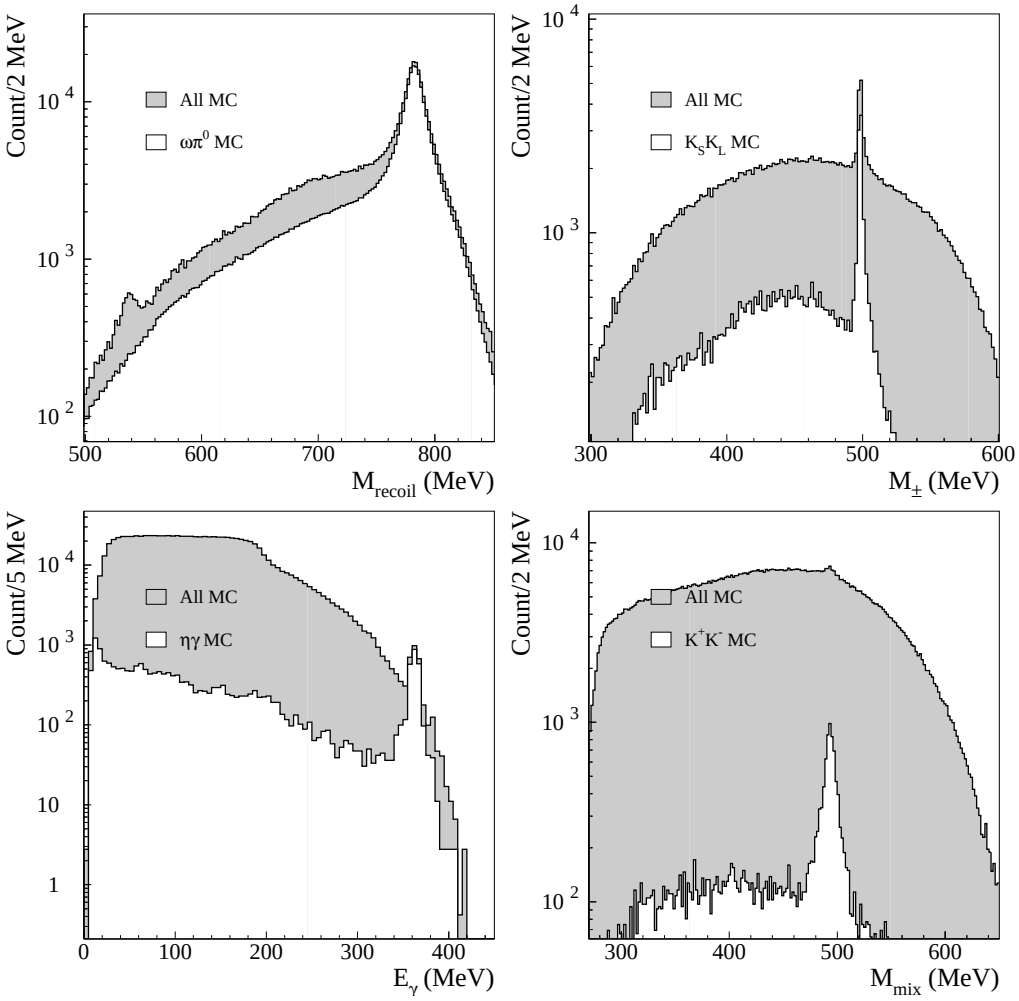

Fig. 6. Distribution obtained with MC at CoM energy of 1019.75 MeV. In the M_{recoil} variable (top-left) the signal peak ($M_{\omega} = 782$ MeV) is clearly visible, together with the small η mass peak at 548 MeV. In the top-right panel, the M_{K^0} is well evident. The E_{γ} distribution (bottom-left) has a peak at 360 MeV due to the radiated photon of $\phi \to \eta\gamma$ events. In the M_{mix} variable a tiny peak around $M_{K^{\pm}}$ is present.

5 MC correction

In this section we discuss all the corrections applied to the MC in order to have a better simulation of the detector response.

5.1 Initial state radiation

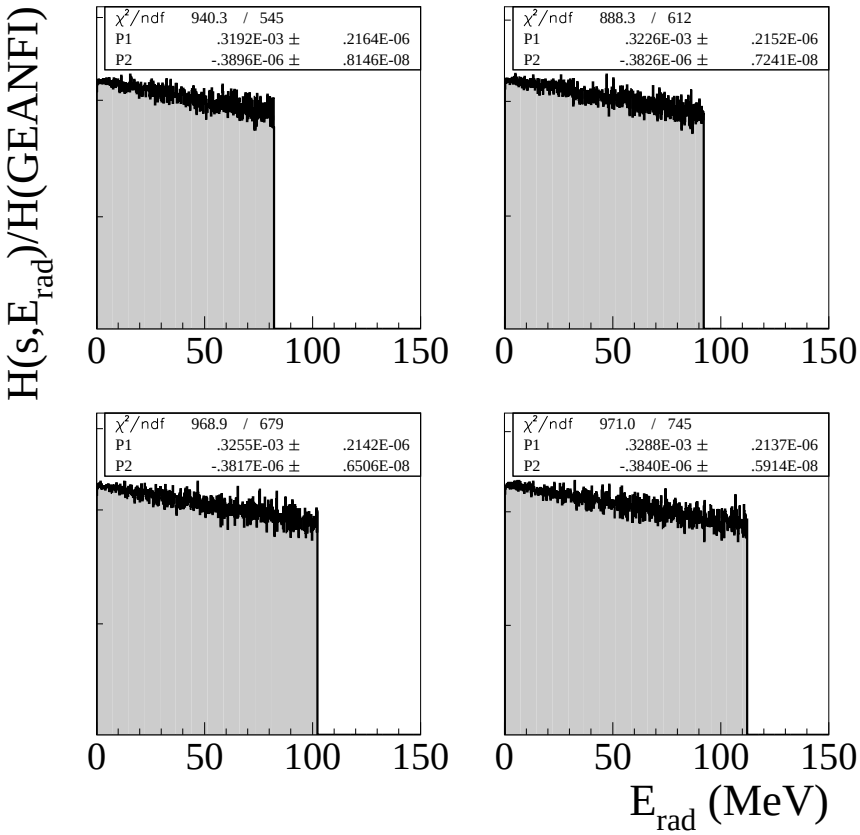

Fig. 7. Radiator shape correction for different center of mass energies: 1000 Mev (top-left), 1010 MeV (top-right), 1020 MeV (bottom-left), 1030 MeV (bottom-right). The correction has been obtained as the ratio of the radiator function inside GEANFI and the radiator kernel calculated at the corresponding center of mass energy. This ratio has been fitted with a linear function ($P_1 + E_{ISR}P_2$) and applied to the signal events.

In our MC generator, the initial state radiation (ISR) is taken into account by applying a simple correction before calling the event generation routine. The maximum energy radiated is fixed at 130 MeV for each value of center of mass energy. Since we observe data at different center of mass energies we apply a global reshaping of the ISR tail as shown in Fig. 7. This correction has been evaluated as the ratio between the radiator function inside our MC generator and the standard radiator used to calculate the radiative correction to the cross section [9,10].

The simulation of EMC in MC does not match perfectly the behavior observed in data. We have used the output of the kinematic fit to check the EMC energy scale response for MC.
In Fig. 8, energy scale and resolution for both Data and MC are shown. Since we have observed a significant difference between Data and MC in the energy scale, we have implemented a dedicated correction to the scale. For the resolution there is no need for any correction.

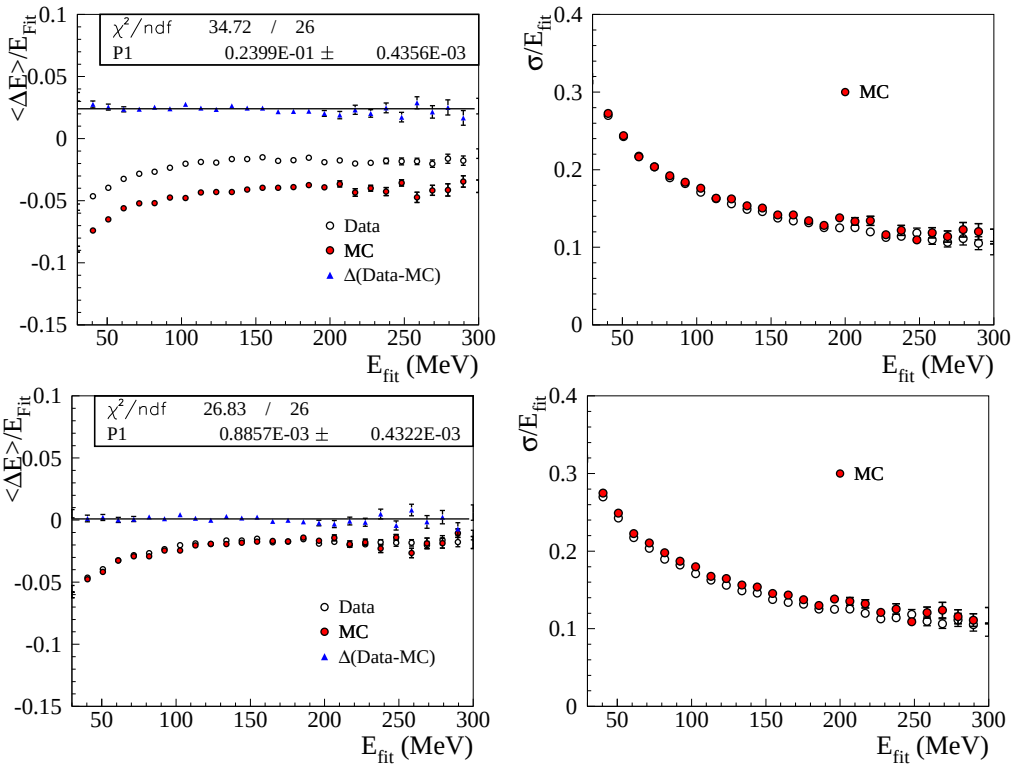

Fig. 8. Top: Energy scale (left) and resolution (right) for clusters as a function of fitted energy of the cluster without correction. Bottom: Energy scale (left) and resolution (right) for clusters after the 2.4% correction on the MC cluster energy.

5.3 Clustering efficiency correction

We have applied the standard cluster efficiency correction already included in the reconstruction [11]. The parametrization of the the correction as a function of the cluster energy is:

$$C_\varepsilon(X) = A\left(1 - \frac{1}{1 + e^{\frac{X - X_0}{\delta}}}\right) \tag{2}$$

where A is the plateau value, X_0 is the central value of the step and δ is proportional to the length of the step (the smaller the steeper).

5.4 Tracking and Vertexing

To study the effect of the tracking/vertexing efficiency we have used an unbiased sample of data (UFO stream [6]) and corresponding MC. We have selected a clean $\phi \to \rho\pi$ sample (purity $> 99\%$) for both data and MC. A complete description of this work can be found in [13].
We have observed that the correction to the tracking efficiency depend on the longitudinal (P_z) and transverse (P_t) momentum of the track. For this reason we use a correction function of P_t in slice of P_z. This properly takes into account the difference between the control sample and our dataset, as shown in Fig. 9, when applying the correction.

The ratio of the Data/MC tracking efficiency as function of P_t, hereafter called the *correction*, has been fitted using the step function (eq. 2) previously described. When the fit with C_ε function has a very poor result, due to the lack of statistics on the border of the $P_t - P_z$ distribution, we use a constant parametrization for the ratio data/MC.
Comparing the fit results of charge separated efficiencies demonstrates that there is no difference due to the charge of the tracks, as can be seen in figure 9.

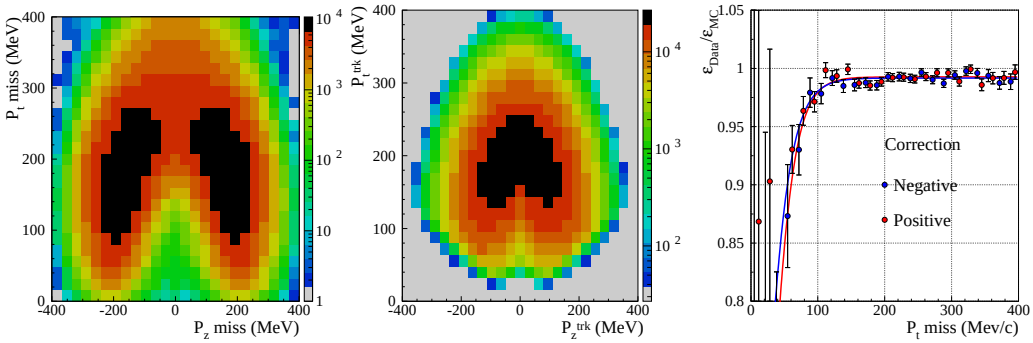

Fig. 9. Spectrum of the missing momentum for the control sample (left) and for signal events in our selection (center). Right: tracking correction for $-20 < P_z < 20$ MeV for the two different charges.

[6] Although the original purpose of the UFO stream [12] was the classification of the unidentified events that are rejected by other streams, after the datarec version 23 the UFO stream contains all KLOE Data events without any kind of classification with a prescale factor of 0.05.

For the vertexing efficiency the agreement between data and MC for 2001-2002 dataset looks very good. However, for the 2005 and then for the *off-peak* data we have a small correction of 0.5%.

6 Acceptance and kinematic fit

The first step of this analysis is the topology selection, requiring events with the expected final state signature:

- only one vertex inside a cylindrical (12 cm height, 4 cm radius) fiducial volume around the interaction point (IP) with only two connected tracks;
- Four neutral clusters (without associated tracks following standard KLOE TCLO algorithm [14]) in the expected time window (TW) defined as $|T_\gamma - R_\gamma/c| < MIN(4 \cdot \sigma_T, 2 \text{ ns})$.

We apply also energy and angular cuts on the clusters in the photon counting in order to minimize machine background and to exclude the region around QCAL: $E_\gamma > 10$ MeV and $22^\circ < \vartheta_\gamma < 158^\circ$.

6.1 Kinematic fit

In order to improve resolution and to increase the background rejection, a global kinematic fit procedure, based on the least squared method, is applied. The free parameters (33 in total) are:

Clusters(5×4): Energy (E_{clu} with a resolution $\Delta E_{clu} = 0.06/\sqrt{E_{clu}(\text{GeV})}$ MeV), time (T_{clu} with a resolution $\Delta T_{clu} = 0.057/\sqrt{E_{clu}(GeV)} \oplus (0.140))$ ns) and position ($\overrightarrow{R}_{clu}$ with a resolution of $\Delta \overrightarrow{R}_{clu} = 1.2$ cm) for each cluster,

Vertex(3): Position of the charged vertex (with a resolution determined with the fit of the vertex position σ_{vtxfit}) ,

Tracks(3×2): Curvature, polar and azimuthal angle (with the resolution determined by the fit of the track connected to the vertex $\sigma_{trkfit|vtxfit}$) for each track ,

Beam(4): Four-momentum of the e^+e^- system (P_ϕ with resolution $\Delta E_\phi = 0.3$ MeV; $\Delta P_x(\phi) = 0.005$ MeV).

The constraints, and thus the number of degrees of freedom (ndf), are 8: total energy-momentum conservation (4) and the requirement $T_\gamma - R_\gamma/c = 0$ for each photon (4).

In order to fully reconstruct the event we have to pair photons with neutral pions. This pairing is performed defining a pseudo-χ^2 as follows:

$$\tilde{\chi}^2 = \left(\frac{M_{\gamma_i\gamma_j} - M_{\pi^0}}{\sigma_{M_{\pi^0}}}\right)^2 + \left(\frac{M_{\gamma_k\gamma_h} - M_{\pi^0}}{\sigma_{M_{\pi^0}}}\right)^2 + \left(\frac{M^i_{3\pi} - M_\omega}{\sigma_{M_\omega}}\right)^2$$

The first two terms are related to gamma pairing, while the last one assigns the π^0 to the ω. The photon combination minimizing the $\tilde{\chi}^2$ is then selected. Although the analysis does not require the omega reconstruction, the insertion of the last term in the $\tilde{\chi}^2$ definition improves the photon pairing efficiency ($0.93 \rightarrow 0.94$).

7 Analysis cuts and Event counting

After acceptance selection, the background composition is dominated by the K_SK_L channel (Tab. 1). Contribution from other channels cannot be neglected. To reduce the $\phi \rightarrow \eta\gamma$ background we use a dedicated cut, *η-cut*, requiring:

$$(E_\gamma^{Max} \in [320; 380] \text{ MeV}) \wedge (M_{3\pi} \in [490; 560] \text{ MeV})$$

where E_γ^{Max} is the energy of the most energetic photon in the event and $M_{3\pi}$ is the invariant mass for the remaining three pions that does not include the π^0 reconstructed with the most energetic photon. The limits for the box are tuned with the MC simulation around the energy of the radiated photon for $\phi \rightarrow \eta\gamma$ events. In Fig. 10-left the *η-cut* is shown for 2001-2002 data. Inside the box the $\eta\gamma$ component is clearly visible.

A residual background component of Bhabha events is rejected using the energy of the two charged tracks in the pion hypothesis and their opening angle (Fig. 10-right). Events with both tracks satisfying:

$$E_{trk} - 450 \cdot \cos\vartheta_\pm - 890. > 0$$

are then rejected (*Bhabha-cut*).

All events surviving those cuts are divided in two classes depending on the value of the χ^2_{Kfit}:

Good-Event: ($\chi^2_{Kfit} < 50$) all events surviving all analysis cuts with low χ^2(signal enriched).

Reject-Event: ($\chi^2_{Kfit} > 50$) all events surviving all analysis cuts with high χ^2 (background enriched).

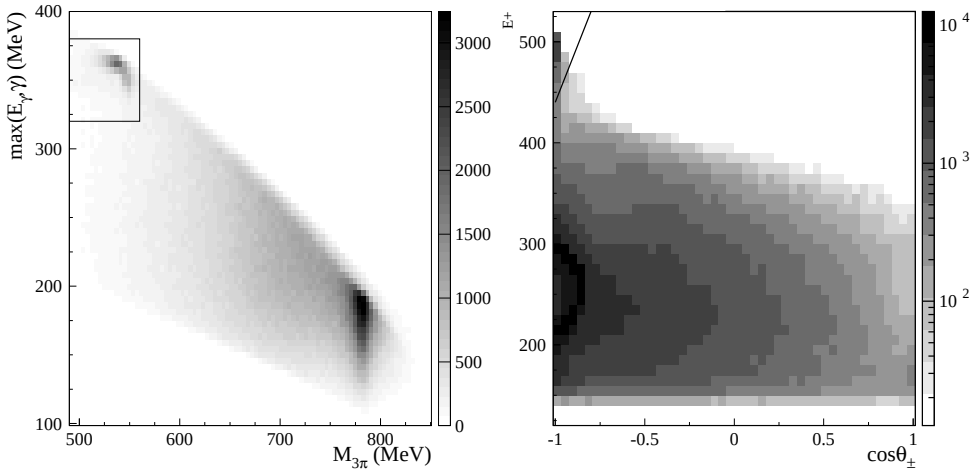

Fig. 10. Background rejection. Left: $M_{3\pi}$ versus the energy of the most energetic photon. The region inside the rectangular box, where the $\phi \to \eta\gamma$ background appears, is excluded (η-*cut*). Right: angle between charged tracks versus the positive charged track energy. The region above the line, where the contamination from Bhabha event is clearly visible, is excluded (*Bhabha-cut*).

Table 1
Signal over background ratio as a function of the analysis stage.

Bkg Channel	ECL	Acceptance	Rejection box	χ^2_{Kfit}
$K_S K_L$	0.30	1.2	4.4	10.
K^+K^-	0.32	14.	40.	55.
$\rho\pi$	0.08	30.	116.	177.
$\eta\gamma$	0.37	22.	336.	833.
Other (ϕ)	9.6	124.	275.	338.

The distribution of χ^2_{Kfit} is shown in Fig. 11, both for low χ^2 values (left) and for the higher tail (right).

Event counting is performed using the standard CERNLIB function HMCMLL [15], fitting data histograms with MC distributions. In the fit we use three different MC components: signal, ϕ backgrounds, $a_1\pi$ background for all value of $\sqrt{s}$. As reference for counting, the distribution of the recoil mass of the reconstructed pions (M_{recoil}, see § 4) has been used. We simultaneously fit both classes [7] of events to determine scale factor of MC components. The scale factor for MC components can be determined from fit results simply by dividing the output of the fit (integral of the distribution for each components) with the integral of the original MC distribution used in the fit. The scale factors are used to normalize signal and background events for both classes in

[7] Using both classes is like a bidimensional fit in which one of the two variables has only two bins.

order to check the agreement between Data and MC as shown in Figs. 12-20.

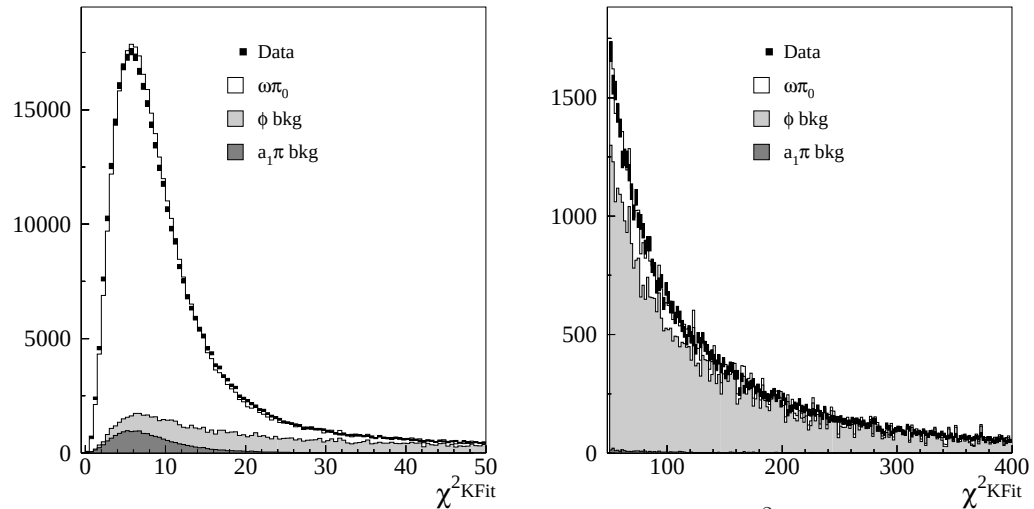

Fig. 11. Comparison between data and MC distribution for χ^2_{Kfit} *Good-Event* (left) and *Reject-Event* (right) selection. The normalization of signal and background are taken from the fit output. In the *Good-Event* selection the total background accounts only for the 14% of the integral.

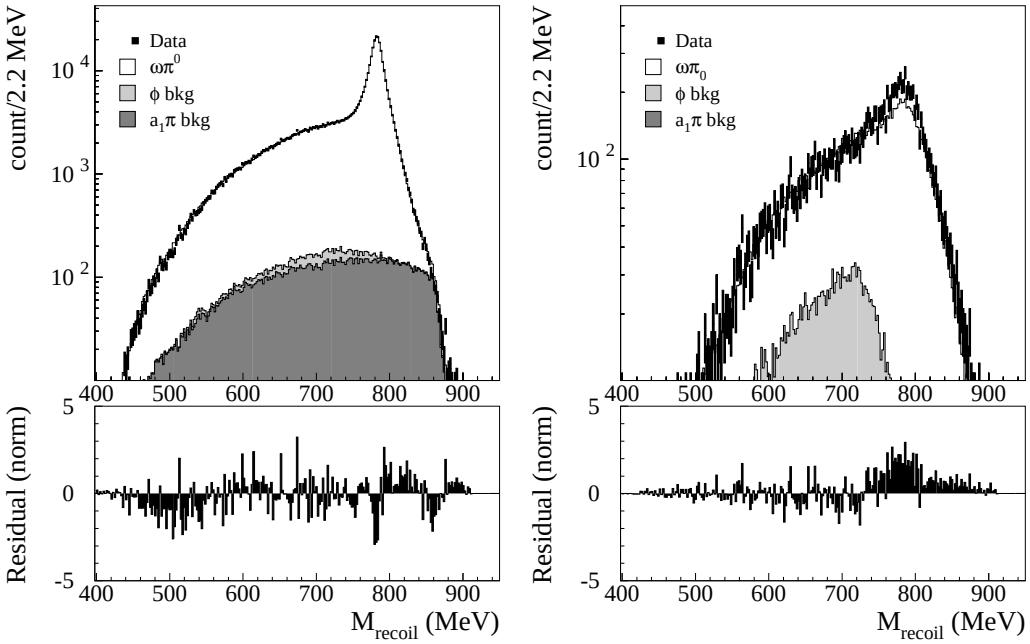

Fig. 12. Top: Fit result at $\sqrt{s} = 1000$ MeV for M_{recoil} in the *Good-Event* selection (left) and for the *Reject-Event* selection (right). Bottom: Normalized residual $(N_{data} - N_{MC}/\sigma_{tot})$.

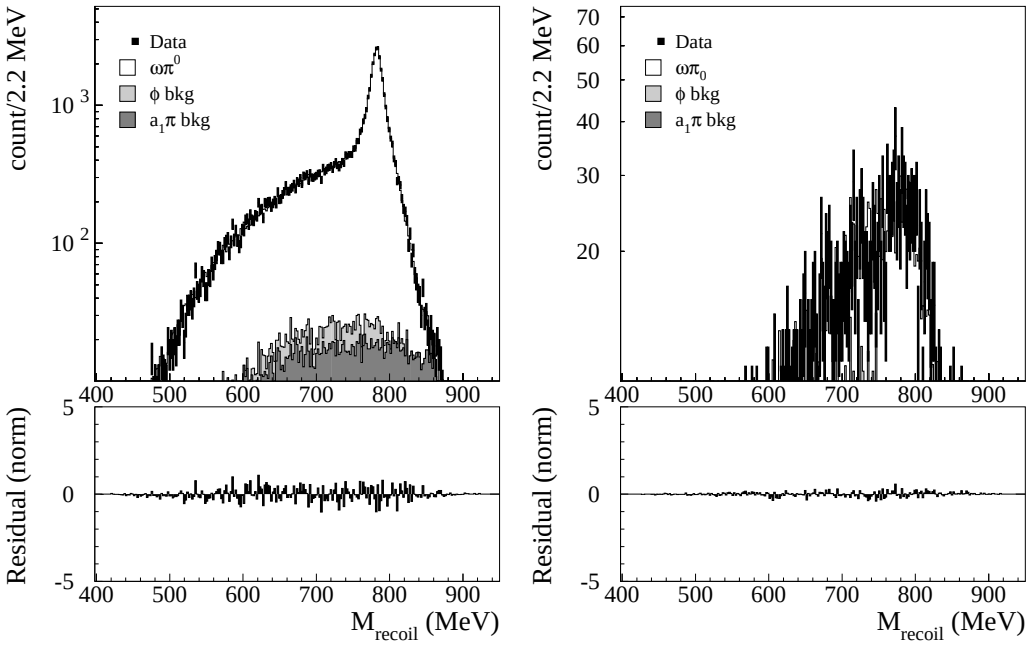

Fig. 13. Top: Fit result at $\sqrt{s} = 1010$ MeV for M_{recoil} in the *Good-Event* selection (left) and for the *Reject-Event* selection (right). Bottom: Normalized residual $(N_{data} - N_{MC}/\sigma_{tot})$.

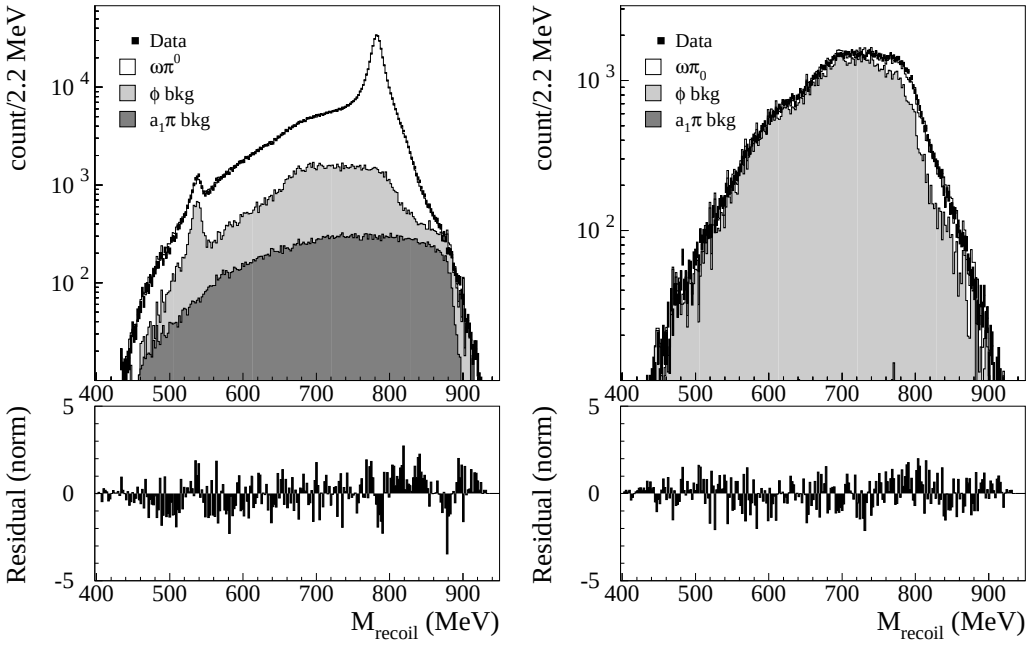

Fig. 14. Top: Fit result at $\sqrt{s} = 1019.75$ MeV for M_{recoil} in the *Good-Event* selection (left) and for the *Reject-Event* selection (right). Bottom: Normalized residual $(N_{data} - N_{MC}/\sigma_{tot})$.

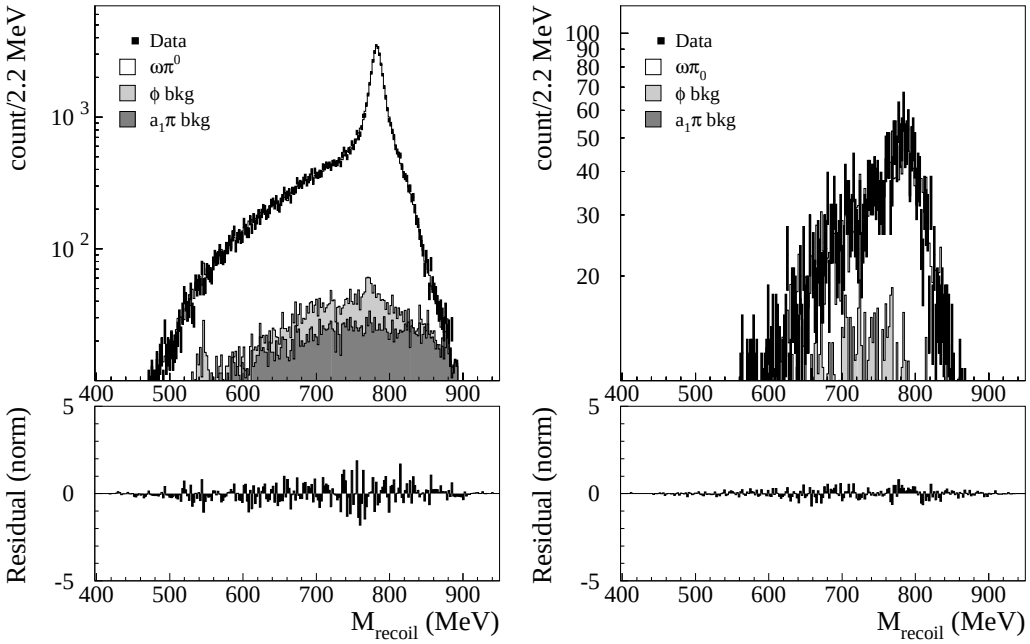

Fig. 15. Top: Fit result at $\sqrt{s} = 1030$ MeV for M_{recoil} in the *Good-Event* selection (left) and for the *Reject-Event* selection (right). Bottom: Normalized residual $(N_{data} - N_{MC}/\sigma_{tot})$.

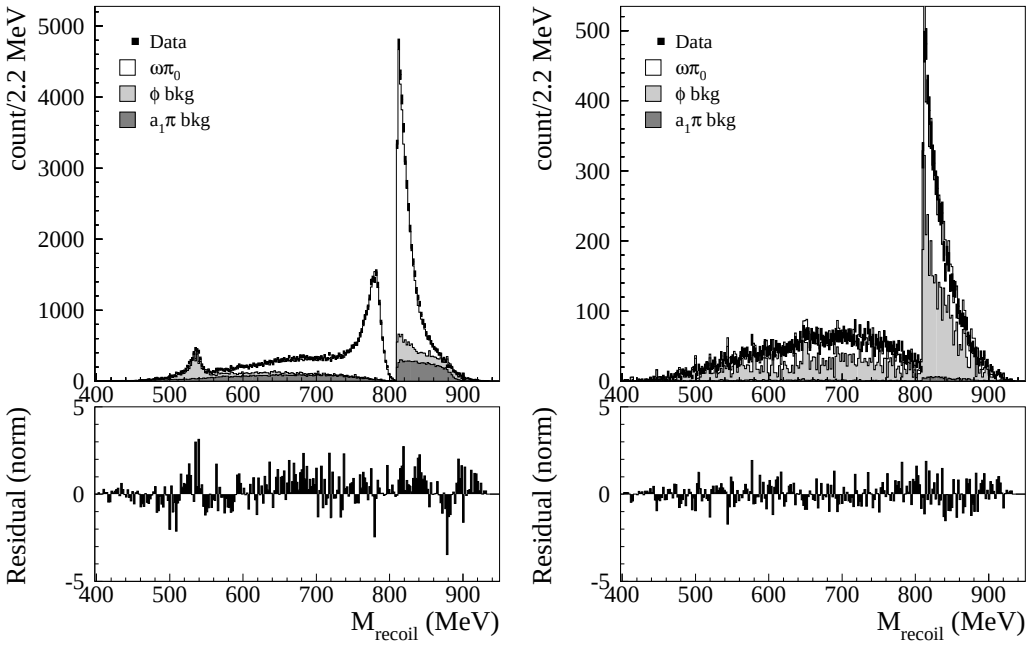

Fig. 16. Data-MC comparison at $\sqrt{s} = 1019.75$ MeV for M_{recoil} when at least one of the two reconstructed recoil masses is above 810 MeV. Left: *Good-Event* event selection, where the greatest part the $a_1\pi$ background is concentrated. Right: *Reject-Event* selection. Bottom: Normalized residual $(N_{data} - N_{MC}/\sigma_{tot})$. The scale factor used to normalize the different MC components are taken from the fit on the M_{recoil} distribution.

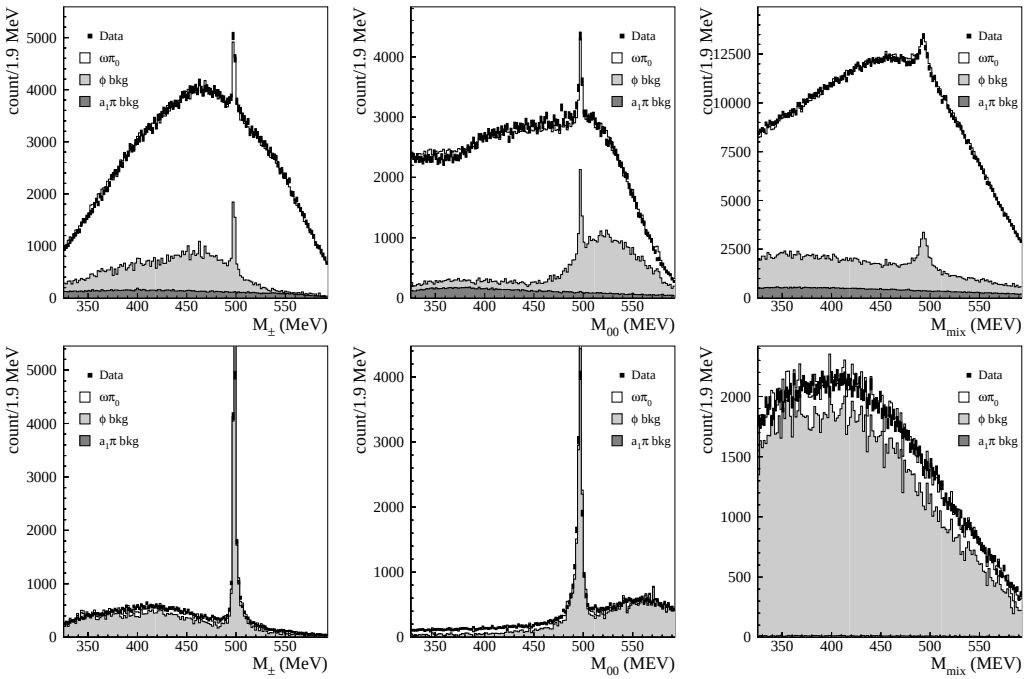

Fig. 17. Data-MC comparison at $\sqrt{s} = 1019.75$ MeV for $M_{\pm}$ (left) M_{00} (center) and M_{mix} (right) for the *Good-Event* selection (top) and for *Reject-Event* (bottom). In the shown region are clearly visible the structures due to kaon background. The scale factor used to normalize the different MC components are taken from the fit on the M_{recoil} distribution.

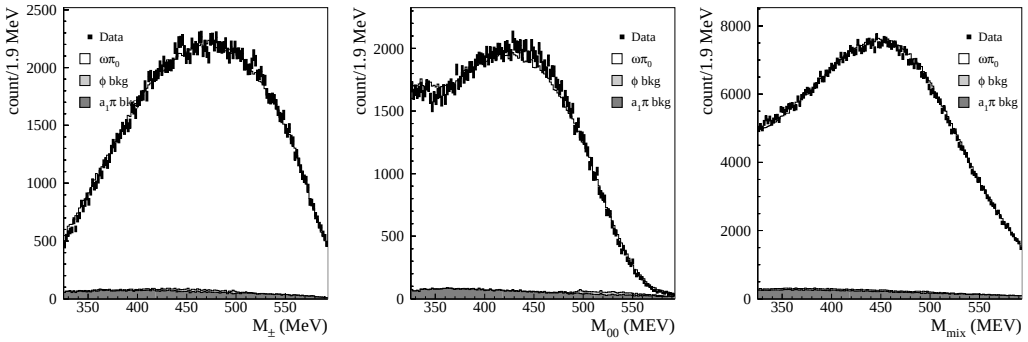

Fig. 18. Data-MC comparison at $\sqrt{s} = 1000$ MeV for $M_{\pm}$ (left), M_{00} (center) and M_{mix} (right) for the *Good-Event* selection. The scale factor used to normalize the different MC components are taken from the fit on the M_{recoil} distribution.

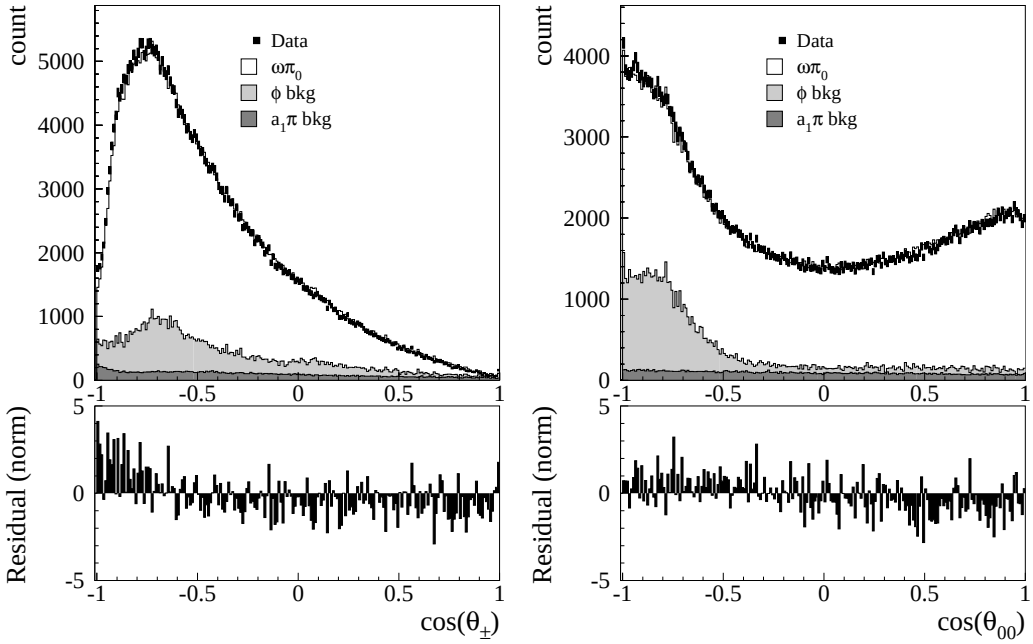

Fig. 19. Top: Data-MC comparison at $\sqrt{s} = 1019.75$ MeV for angle between charged tracks in the ω rest frame (left) and for the reconstructed π^0 in ϕ rest frame (right) in the *Good-Event* selection. Bottom: Normalized residual $(N_{data} - N_{MC}/\sigma_{tot})$. The scale factor used to normalize the different MC components are taken from the fit on the M_{recoil} distribution.

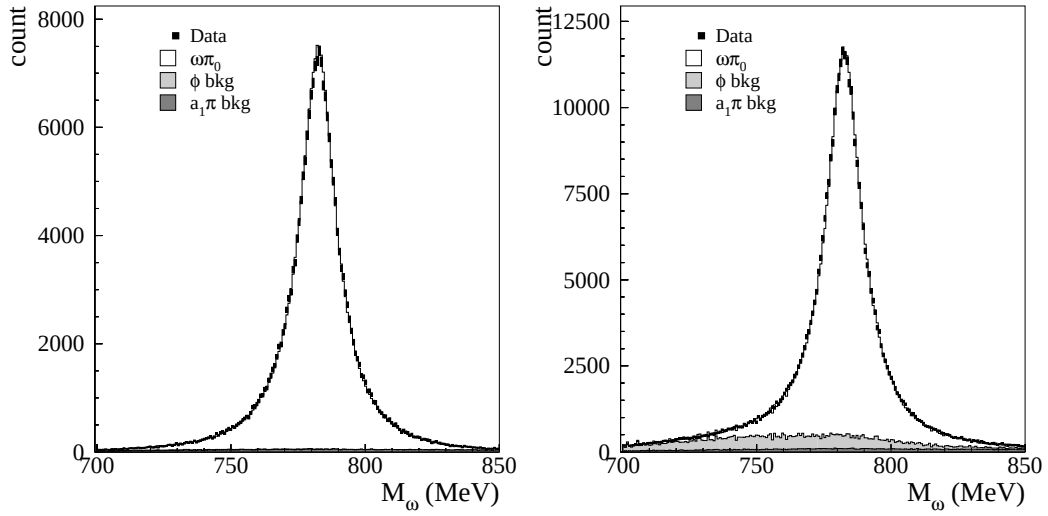

Fig. 20. Data-MC comparison at $\sqrt{s} = 1000$ MeV (left) and $\sqrt{s} = 1019.75$ MeV (right) for the reconstructed ω mass. Events are from *Good-Event* selection. The scale factor used to normalize the different MC components are taken from the fit on the M_{recoil} distribution. The peak value, determined via fit with a Breit-Wigner function, is: 782.3 MeV.

Table 2
Contribution to the analysis efficiency (ε_{ANA}) for MC events generated at $\sqrt{s}$=1019.75 MeV. In the right column are the efficiency values as a function of the analysis stage.

Cut	$\varepsilon_{cut}(\%)$		
Trigger	99.06	$\pm$	-
ECL	57.12	$\pm$	0.02
Acceptance	41.69	$\pm$	0.02
Analysis cuts	37.87	$\pm$	0.02

7.1 Efficiency

The total efficiency is used in the analysis as a function of $\sqrt{s}$ to get the right normalization for the cross section. In Fig. 21 the entire energy range is shown. The observed fluctuation of the efficiency for the *on-peak* data is due to the different data tacking condition during 2001-2002 that are packed together in the same bin of $\sqrt{s}$.
The mean value of the efficiency is around 38%.

In the Tab. 2, the scaling of efficiency as a function of the analysis stage is shown. In the table, only the events coming in the bin 1019.75 MeV of $\sqrt{s}$ are considered. The event classification (ECL) seems to be the most important contribution. However, when evaluating the ECL conditional efficiency at the end of the analysis chain, the ECL term accounts for a conditional efficiency of only $\sim 92\%$.

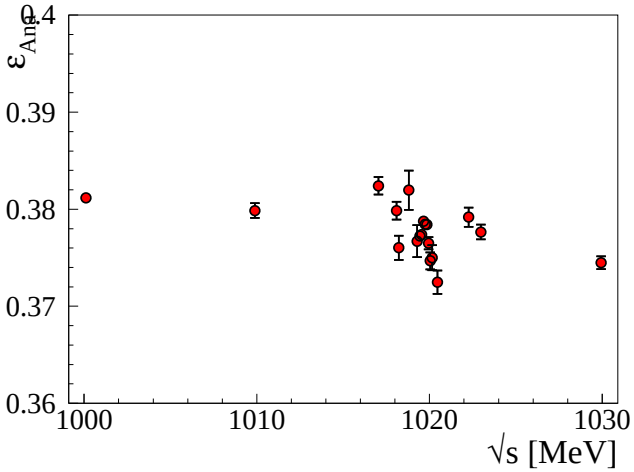

Fig. 21. MC efficiency as a function of $\sqrt{s}$. The observed difference between *on-peak* and *off-peak* point is due to the different run condition.

8 Systematics on absolute normalization

The evaluation of the systematics connected to the absolute normalization (e.g. efficiency and luminosity) is discussed in this section. While for the luminosity we rely on theoretical uncertainty of the very large angle Bhabha generator (BABAYAGA [16]), concerning the efficiencies we have considered different sources of systematics that can be divided in three main categories: preselection, resolution effects and reconstruction effects. Since we have charged pions in the final state, we have also considered the effect of the correction induced by the final state radian (FSR).

8.1 Preselection

The preselection consists of a trigger request, cosmic veto and FILFO filter. To evaluate the corresponding efficiency and systematics, we use MC signal events surviving both acceptance and analysis cuts. Losses due to trigger selection and FILFO are found to be negligible and will be ignored. For the cosmic veto (CV) we obtain a total efficiency of:

$$\varepsilon_{CV}^{MC} = (99.85 \pm 0.02)\%$$

The CV efficiency also has been checked directly on data. We evaluate the CV losses with 2001 data, using prescaled events. Since in 2002 there was the T3 filter running, recovering some of the CV losses, we keep the same correction of 2001, disregarding the events with a CV flag in data. The total efficiency correction to be applied on data is found to be:

$$\varepsilon_{CV}^{DATA} = (99.59 \pm 0.01)\%$$

The discrepancy between data and MC is taken as systematic error.

$$\delta_{CV} = \frac{\varepsilon_{CV}^{MC} - \varepsilon_{CV}^{DATA}}{\varepsilon_{CV}^{DATA}} = 0.3\%$$

8.2 Resolution

The systematics connected to the resolution is due to the possible fluctuation of analysis efficiency induced by the resolution of the variables used for selection (e.g. The minimum energy of the photon for acceptance selection).
To analyse those effects we have considered the relative variation of the efficiency around its reference value due to a 1σ displacement of the variable used to define a cut.

8.2.1 Acceptance

The sample selection is performed requiring two tracks connected to the primary vertex and four photons inside an angular region $22° < \vartheta_\gamma < 158°$ with energy greater than 10 MeV. To evaluate the error on these requirements we have to take into account the effect of the EMC energy and angular resolution, shown in Fig. 22. We quote systematics as the relative variation in efficiency:

$$\delta_{acc}(X) = \left. \frac{|\varepsilon_{Acc}(X + \Delta X) + \varepsilon_{Acc}(X - \Delta X)|}{\overline{\varepsilon}_{Acc}(X)} \right|_{X=\left\{E_{clu}^{min};\vartheta_{clu}^{min}\right\}}$$

Summing in quadrature these two contributions we obtain:

$$\delta_{acc} = 0.3\%$$

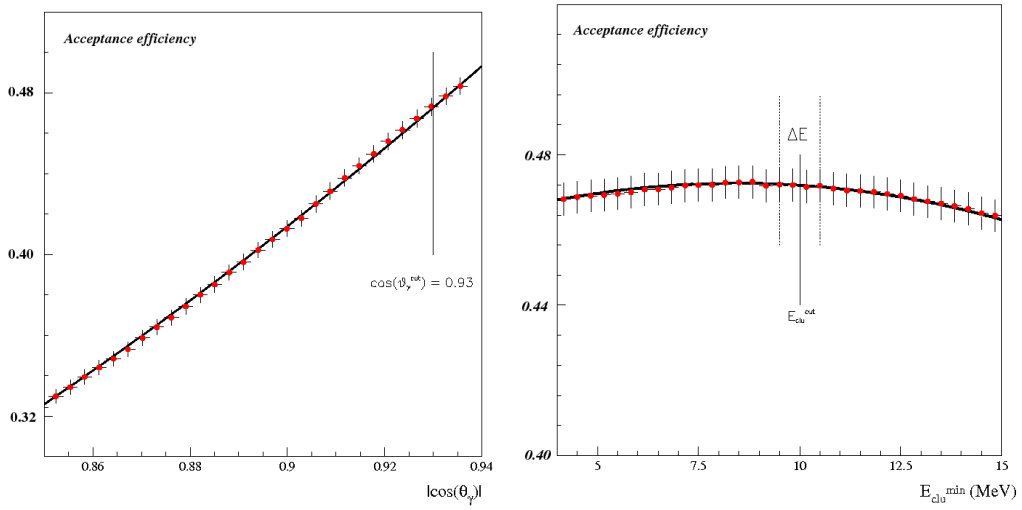

Fig. 22. Left: acceptance efficiency as a function of angular cut. Red dots are MC events, while the black line is the fitting function used to determine the variation with angular resolution. Right: acceptance efficiency as a function of the minimum cluster energy. Red dots are MC events, while black line is the fitting function used to determine the variation with cluster energy resolution.

Moreover, we have also considered the effect of the miscalibration in angular distribution and energetic response between Data and MC. The impact of these two effects will be discussed for the final systematics.

8.2.2 Background rejection

After the sample selection, we apply two cuts, for a selective rejection of the background ($\eta\gamma$ and Bhabha). To compute the related systematics, we have changed the *η-box* (see § 7) and the position of the *Bhabha-filter* cut. As in the previous case, we quote the relative variation due to resolution as systematics:

$$\delta_{cuts} = 0.3\%$$

8.3 Event reconstruction

In this section, we discuss the systematic effect due to the difference between data and MC in the reconstruction of the events.

8.4 FSR

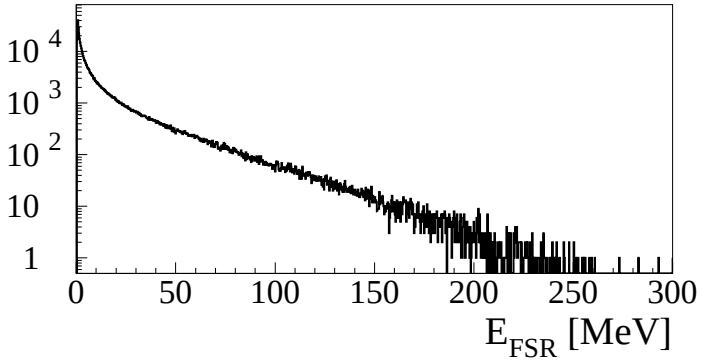

Fig. 23. Tail of the FSR photons obtained with PHOTOS. Only photons with energy greater than 10 MeV (0.7% of the total) of the total radiated events can contribute to the efficiency correction.

We have studied the contribution of final state radiation (FSR) by including PHOTOS [17] in our signal analysis. To evaluate the systematics induced by the FSR photons, we have calculated the variation in the selection efficiency due to these photons. The radiated spectra is shown in Fig. 23. We quote as systematics due to FSR a relative contribution of 0.2%. Negligible fluctuation of this contribution are found as a function of center of mass energy.

8.5 Summary of systematics for counting

The summary of systematic errors on the absolute normalization is reported in Tab. 3. The total systematic error of 1% will be added in quadrature to the counting. Other effects, like tracking, vertexing, and angular distribution of photons, will be treated separately in the following paragraphs.

Table 3
Summary table of systematics.

Source	$\delta_\varepsilon/\varepsilon$
Cosmic Veto	0.3 %
Acceptance	0.3 %
Analysis cuts	0.3 %
FSR	0.2 %
Luminosity	0.5 %
Total	0.75 %

9 Fit to the $\sqrt{s}$-dependence of the visible cross sections

In the energy region below 1.4 GeV, the $\pi^+\pi^-\pi^0\pi^0$ production cross section related to the VMD term is dominated by the non resonant process $e^+e^- \to \rho/\rho' \to \omega\pi^0$. However at $\sqrt{s} \sim M_\phi$, a sizable contribution from the OZI and G-parity suppressed decay $\phi \to \omega\pi^0$ is expected. The coexistence of all these effects appears as an interference pattern in the energy dependence of the cross section around the ϕ mass.
The cross section is usually written in the form [18]:

$$\sigma^{4\pi}(\sqrt{s}) = \sigma^{4\pi}_{nr}(\sqrt{s}) \cdot \left| 1 - Z_{4\pi} \frac{M_\phi \Gamma_\phi}{D_\phi} \right|^2 \tag{3}$$

where $\sigma^{4\pi}_{nr}(\sqrt{s})$ is the bare cross section for the non resonant process, $Z_{4\pi}$ is the complex interference parameter [8] (i.e. the ratio between the ϕ decay amplitude and the non resonant process), while M_ϕ, Γ_ϕ and D_ϕ are mass, width and the inverse propagator of the ϕ meson respectively.
For the non resonant process, a linear dependence $\sigma^{4\pi}_{nr}(\sqrt{s}) = \sigma^{4\pi}_0 + \sigma'_{4\pi}(\sqrt{s} - M_\phi)$ is used. The slope $\sigma'_{4\pi}$ is an important parameter of the fit and the wider range in $\sqrt{s}$ available with *off-peak* data is crucial to reliably determine it.
The measured values of the $\omega\pi^0$ visible cross section are listed in Tab. 4. The errors account for both statistical and systematic uncertainties from Tab. 3.
The free parameters of the fit are $\sigma^{4\pi}_0$, $\Re(Z)$, $\Im(Z)$ and σ', where $\sigma^{4\pi}_0$ represents the cross section for the process under study at the ϕ mass resonance.
The fit to the visible cross section has been performed through the convolution

[8] Index 4π specify that this interference parameter is related to $\pi^+\pi^-\pi^0\pi^0$ final state and could not be directly related to the neutral one.

Table 4
Visible cross section as a function of center of mass energy ($\sqrt{s}$) for $\pi^+\pi^-\pi^0\pi^0$events. The cross section errors includes also the systematics on the absolute scale normalization from Tab. 3

$\sqrt{s}$	$L_{\rm int}(nb^{-1})$	Count [P(χ^2_{count})%]	ε	$\sigma^{4\pi}_{vis}$
1000.10	101795	221917 ± 562 [13]	0.3812 ± 0.0003	5.72 ± 0.05
1009.90	11019	25968 ± 172 [52]	0.3799 ± 0.0008	6.20 ± 0.06
1017.20	7417	16209 ± 171 [93]	0.3824 ± 0.0009	5.71 ± 0.08
1018.15	10455	22167 ± 158 [99]	0.3785 ± 0.0007	5.60 ± 0.06
1019.30	2167	4799 ± 90 [99]	0.3767 ± 0.0017	5.88 ± 0.12
1019.45	26139	58077 ± 340 [68]	0.3773 ± 0.0005	5.89 ± 0.06
1019.55	41808	93596 ± 445 [24]	0.3774 ± 0.0004	5.93 ± 0.05
1019.65	75735	171571 ± 888 [17]	0.3788 ± 0.0003	5.98 ± 0.05
1019.75	142975	326774 ± 872 [16]	0.3784 ± 0.0002	6.04 ± 0.05
1019.85	111335	256008 ± 1248 [08]	0.3784 ± 0.0002	6.08 ± 0.05
1019.95	15350	35850 ± 262 [99]	0.3765 ± 0.0006	6.20 ± 0.07
1020.05	7720	17971 ± 166 [97]	0.3747 ± 0.0009	6.21 ± 0.08
1020.15	3506	8190 ± 132 [99]	0.3750 ± 0.0013	6.23 ± 0.11
1020.45	4049	9657 ± 116 [99]	0.3725 ± 0.0012	6.41 ± 0.09
1022.30	6169	16931 ± 140 [98]	0.3792 ± 0.0010	7.24 ± 0.08
1023.00	10585	29611 ± 177 [95]	0.3776 ± 0.0008	7.41 ± 0.07
1029.95	11472	33681 ± 186 [80]	0.3745 ± 0.0007	7.84 ± 0.07

of eq. 3 with the initial state radiation as follows:

$$\sigma^{4\pi}_{vis}(\sqrt{s}) = \int_{thr}^{\sqrt{s}} \sigma^{4\pi}(x) H_{RAD}(x, \sqrt{s}) dx$$

where H_{RAD} is the radiator function [9,10] which gives the probability that ISR photons are emitted from the e^+e^- pair thus lowering the beam energy from $\sqrt{s}$ to x. We have also performed a further convolution with the beam energy spread (BES) of 300 KeV according to [19].
The results of the fit are summarized in Tab. 5 and the visible cross section is shown in Fig. 24.

Table 5
Fit result. Results are presented as fitted values followed by statistics determined by the fit. The right part of the table is the correlation matrix (in percentile) for the fit parameters.

Fit parameters - P(χ^2_{fit})=98%				Correlation matrix			
$\sigma_0^{4\pi}$ (nb)	7.89	$\pm$	0.06	-	-34	-81	79
$\Re(Z)$	0.109	$\pm$	0.007	-34	-	6	-46
$\Im(Z)$	-0.103	$\pm$	0.004	-81	6	-	-45
σ' (nb/MeV)	0.063	$\pm$	0.003	79	-46	-45	-

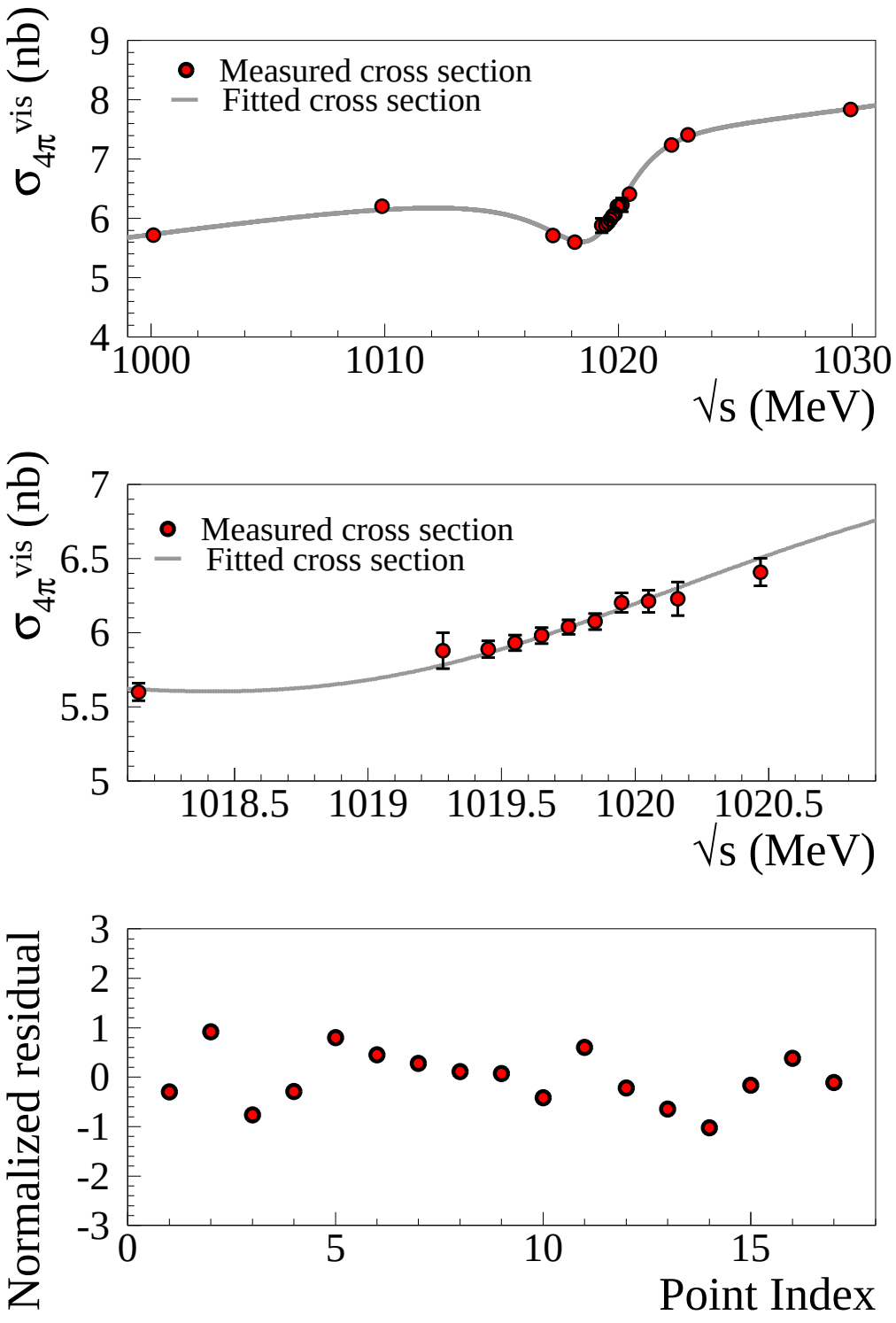

Fig. 24. Top: visible cross section for $e^+e^- \to \omega\pi^0 \to \pi^+\pi^-\pi^0\pi^0$. Points are experimental results and solid line is the fit result ($\chi^2/n.d.f. = 4.78/(17-4)$ with a corresponding probability of 98%). Center: ϕ resonance region zoomed. Bottom: normalized residual of the fit as a function of the index of the point.

10 Final systematics

We have studied the stability of our determination of cross section parameters by varying the analysis procedure. In the following paragraphs, we discuss each considered source of systematic error.

To check the calibration of EMC simulation and the goodness of the MC generator, we have considered:

- Minimum cluster energy to accept the cluster in the event topology scanned between 7 MeV and 19 MeV with step size of 3 MeV. The default value is 10 MeV;
- Minimum azimuthal angle to accept the cluster in the event topology scanned from 20 to 30 with step size of 2 degree. The default value is 20 degree;
- Maximum size of the time window to accept the cluster scanned in the range 3-5 σ_t. The default value is 4 σ_t

With these three cuts, the total efficiency ranges between 28% and 40%. The variations observed are shown in the Fig. 25, 26 and 27.

To check the tracking-vertexing efficiency correction curves, we have used two two different methodologies: moving by $\pm 1\sigma$ the parameter that describes the correction as a function of P_t and using different curves (e.g. varying the maximum angle between missing momentum and track momentum in the control sample).

We have also varied the cut on χ^2_{Kfit} that defines the two classes *Good-Event* and *Reject-Event* in order study the variation as a function of the background content in the two classes. We have used six different cuts ranging between 10 to 70. The total efficiency ranges between 25% and 38%. The variation observed are shown in the Fig. 28.

To check the influence of the MC shape on the counting, we have used different sets of distributions for the *Reject-Event* selection to perform the counting fit for each of the previous defined variations. The variations observed are shown in the Fig. 29 only for the default set of cuts.

We quote as systematics the quadratic sum of the r.m.s.'s obtained in each class of variations considered [9] for each cross section parameters . To accept value in the r.m.s. calculation we require a minimal χ^2 probability (10%) for the output of the cross section fit. The complete list of the systematics error are reported in Tab. 6 and shown in Figs. 25-29. The final results are reported in Tab. 7 and shown in Fig. 30.

[9] $\delta_X = \delta_X(1) \oplus ... \oplus \delta_X(n)$

Table 6
Final systematics on the cross section parameters divided per cause. The total value is calculated as the quadrature of all the contribution.

Cause	σ_0 (nb)	$\Re(Z)$	$\Im(Z)$	σ' (nb/MeV)
Fit distribution	0.005	0.0011	0.0006	0.0005
E_{clu}^{min}	0.023	0.0008	0.0006	0.0005
ϑ_{clu}^{min}	0.047	0.0013	0.0017	0.0007
σ_t	0.046	0.0033	0.0025	0.0005
$\chi^2_{Kfit}cut$	0.013	0.0020	0.0007	0.0005
$\varepsilon_{trk/vtx}$	0.017	0.0004	0.0010	0.0004
Total	0.073	0.0043	0.0034	0.0013

Moreover, we also have exploited a parametrization different from eq. 3 to describe the non resonant part of the cross section. Following the ref. [18], we have used a alternative parametrization for the non resonant part of the cross section:

$$\sigma_{nr}^{4\pi}(E) = \frac{4\pi\alpha^2}{E^3}\left(\frac{g_{\rho\omega\pi}}{f_\rho}\right)^2 \left|\frac{m_\rho}{D_\rho} + A\frac{m_{\rho'}}{D_{\rho'}}\right|^2 P_f(E) \tag{4}$$

where $D_{\rho(\rho')}$ is the inverse propagator of $\rho(\rho')$ meson, A is a real parameter expressing the relative contribution to the $\omega\pi^0$ intermediate state passing trough the two vector mesons, and $P_f(E)$ is the weight of the phase space as a function of the total energy E. In this case, we have substituted the slope parameter $\sigma'_{4\pi}$ with the A parameter. The interference parameter is the same (the interference part of the cross section is unchanged). To to have a direct comparison with the constant term, we have written the fitting function as eq. 4 divided by its value at m_ϕ.

The results is in complete agreement with those obtained by the parametrization of eq. 3: σ_0 7.95 $\pm$ 0.05, $\Re e(Z)$ 0.107 $\pm$ 0.006, $\Im m(Z)$ -0.104 $\pm$ 0.004.

Table 7
Final results. Results are presented as fitted values followed by statistical errors determined by the fit and systematic error.

Fit parameters					
$\sigma_0^{4\pi}$ (nb)	7.89	$\pm$	0.06	$\pm$	0.07
$\Re(Z)$	0.109	$\pm$	0.007	$\pm$	0.004
$\Im(Z)$	-0.103	$\pm$	0.004	$\pm$	0.003
σ' (nb/MeV)	0.063	$\pm$	0.003	$\pm$	0.001

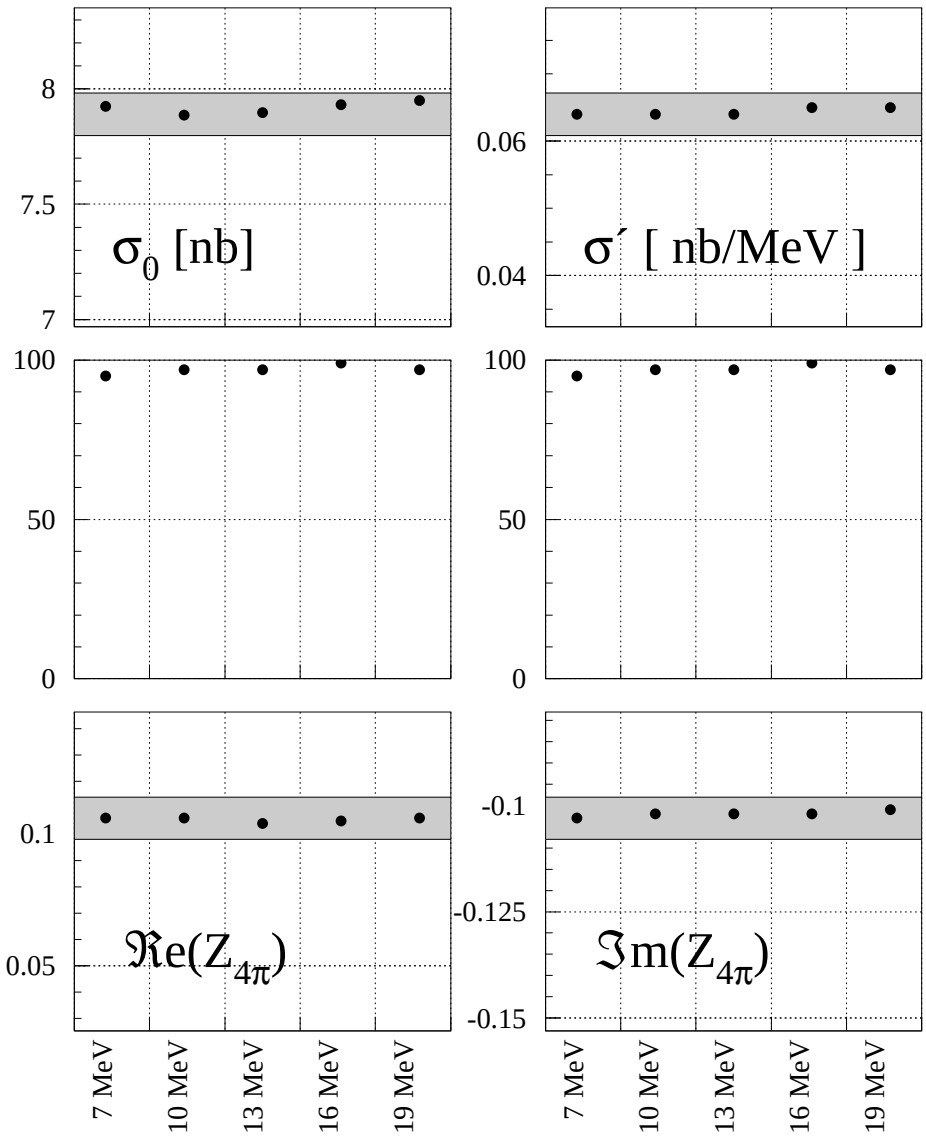

Fig. 25. Variation of the cross section fit results due to variation of minimum cluster energy requirement in the preliminarily selection. Top-left σ_0, top-right: σ', bottom-left: $\Re e(Z)$, bottom-right: $\Im m(Z)$. In the center plots, the value of χ^2 probability of the cross section fit is shown. The gray band represent the full error on the cross section parameters (stat $\oplus$ syst).

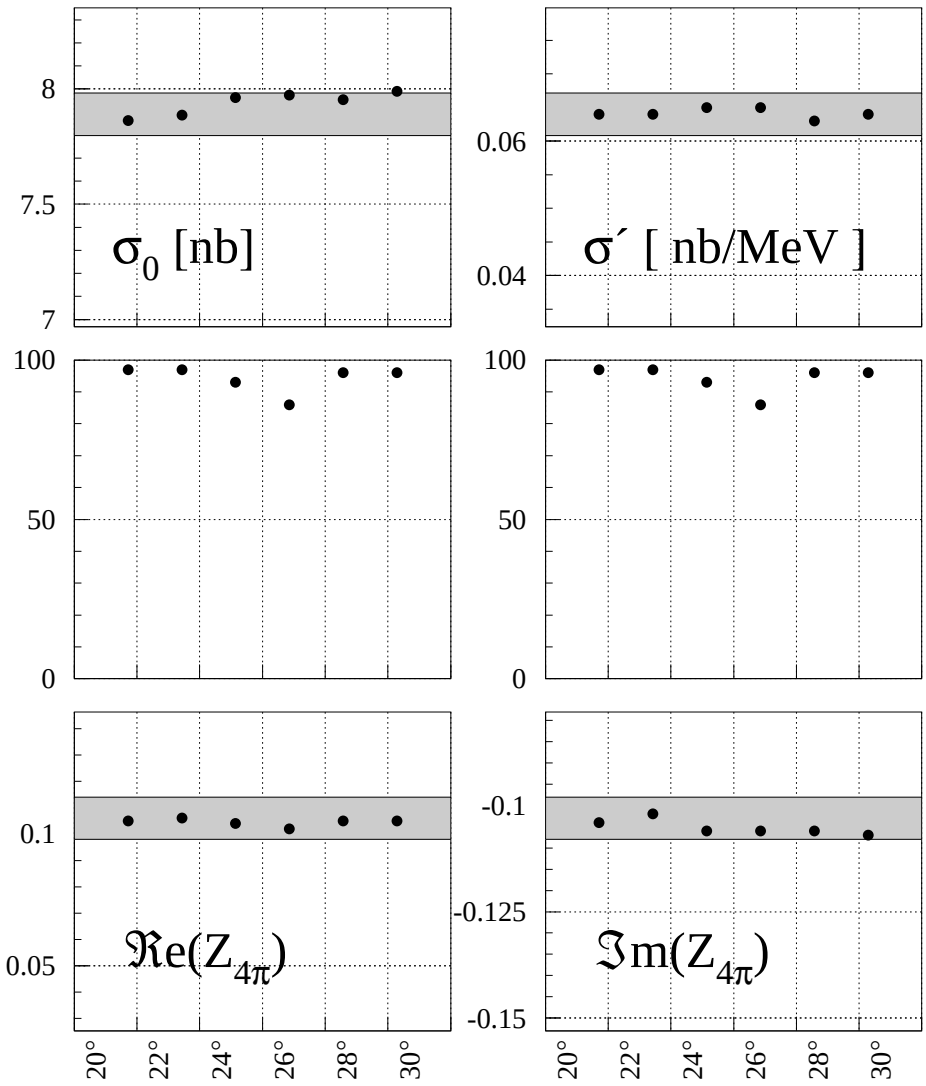

Fig. 26. Variation of the cross section fit results due to variation of minimum azimuthal angle requirement in the preliminary selection. Top-left σ_0, top-right: σ', bottom-left: $\Re e(Z)$, bottom-right: $\Im m(Z)$. In the center plots, the value of χ^2 probability of the fit is shown. The gray band represents the full error on the cross section parameters (stat $\oplus$ syst).

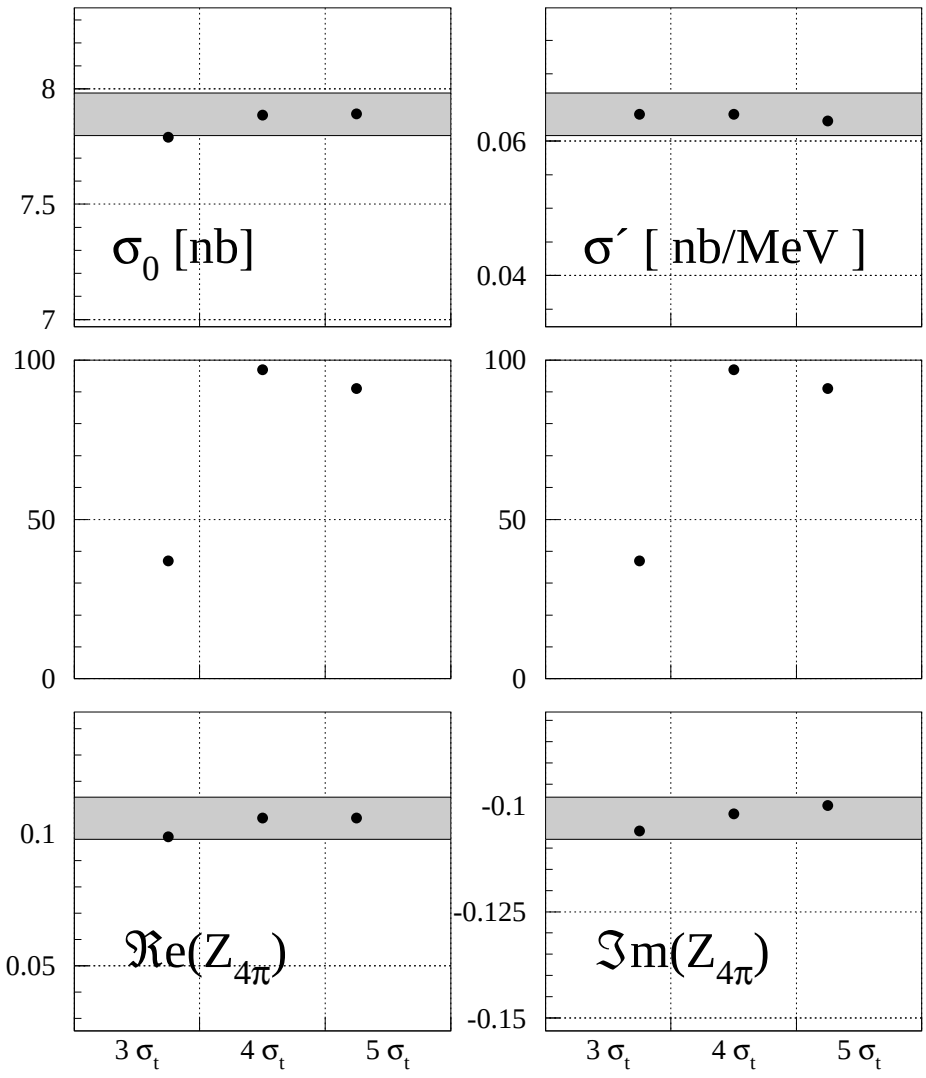

Fig. 27. Variation of the cross section fit results due to variation of size of the time window in the preliminary selection. Top-left σ_0, top-right: σ', bottom-left: $\Re e(Z)$, bottom-right: $\Im m(Z)$. In the center plots, the value of χ^2 probability of the fit is shown. The gray band represents the full error on the cross section parameters (stat $\oplus$ syst).

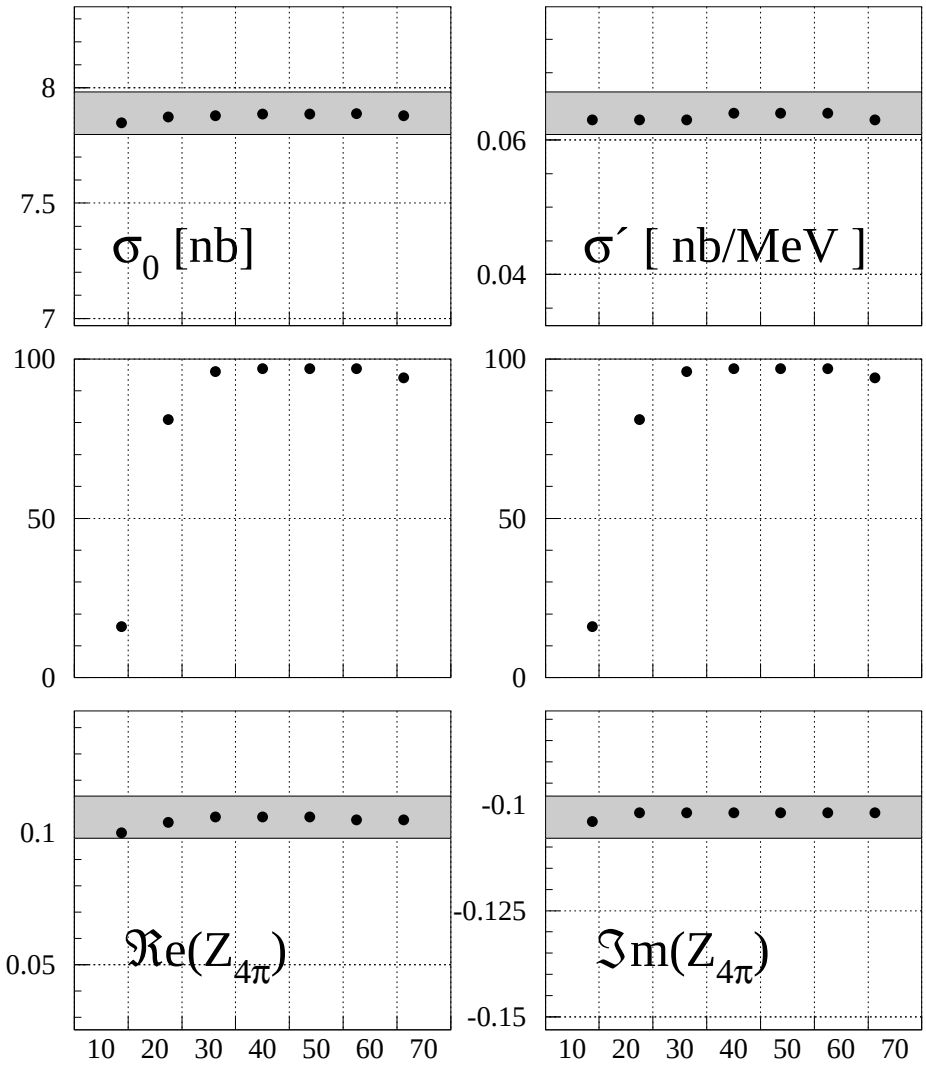

Fig. 28. Variation of the cross section fit results due to variation of the cut on χ^2_{KFit}. Top-left σ_0, top-right: σ', bottom-left: $\Re e(Z)$, bottom-right: $\Im m(Z)$. In the center plots, the value of χ^2 probability of the fit is shown. The gray band represents the full error on the cross section parameters (stat $\oplus$ syst).

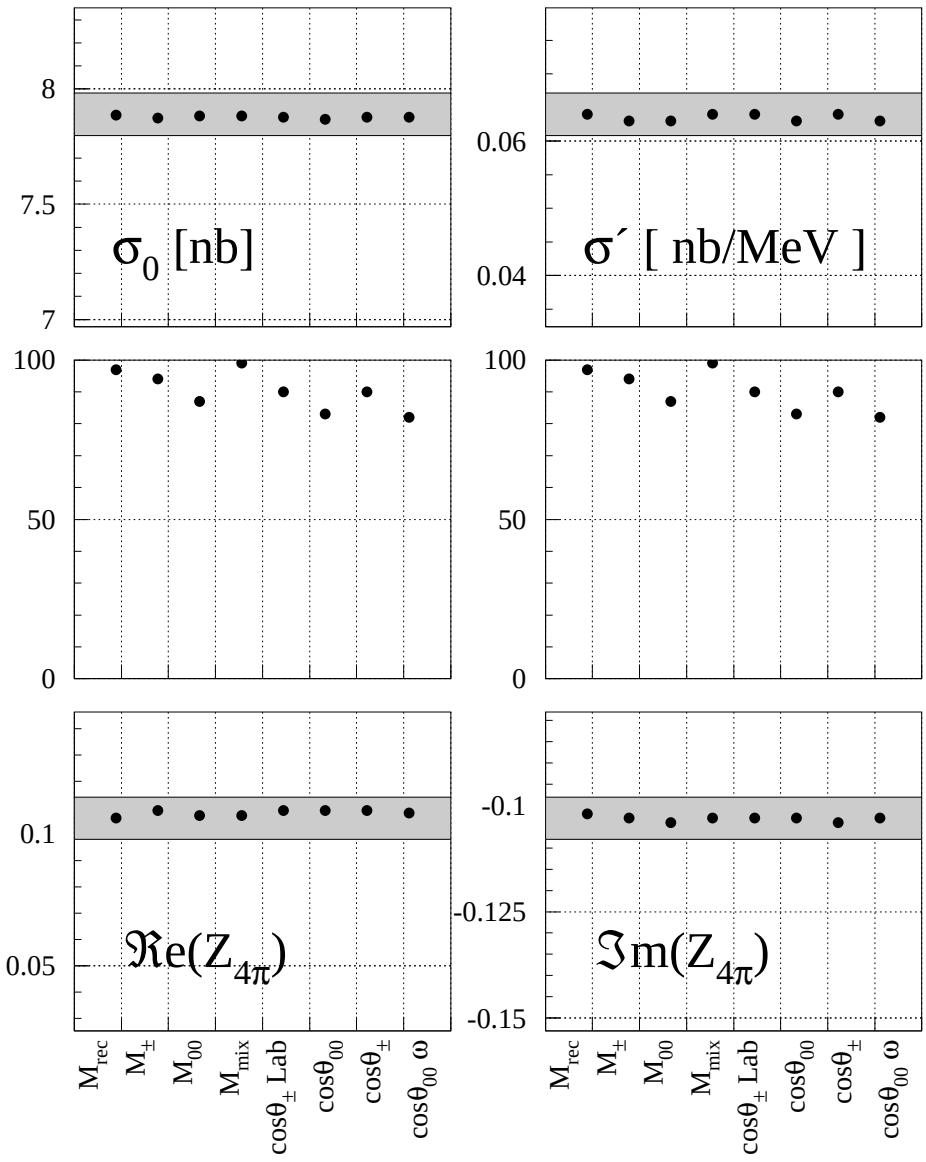

Fig. 29. Variation of the cross section fit results due to variation on the physical distribution used in the counting fit. The label refers to the distribution chosen for the *Reject-Event* class. Top-left σ_0, top-right: σ', bottom-left: $\Re e(Z)$, bottom-right: $\Im m(Z)$. In the center plots, the value of χ^2 probability of the fit is shown. The gray band represents the full error on the cross section parameters (stat $\oplus$ syst).

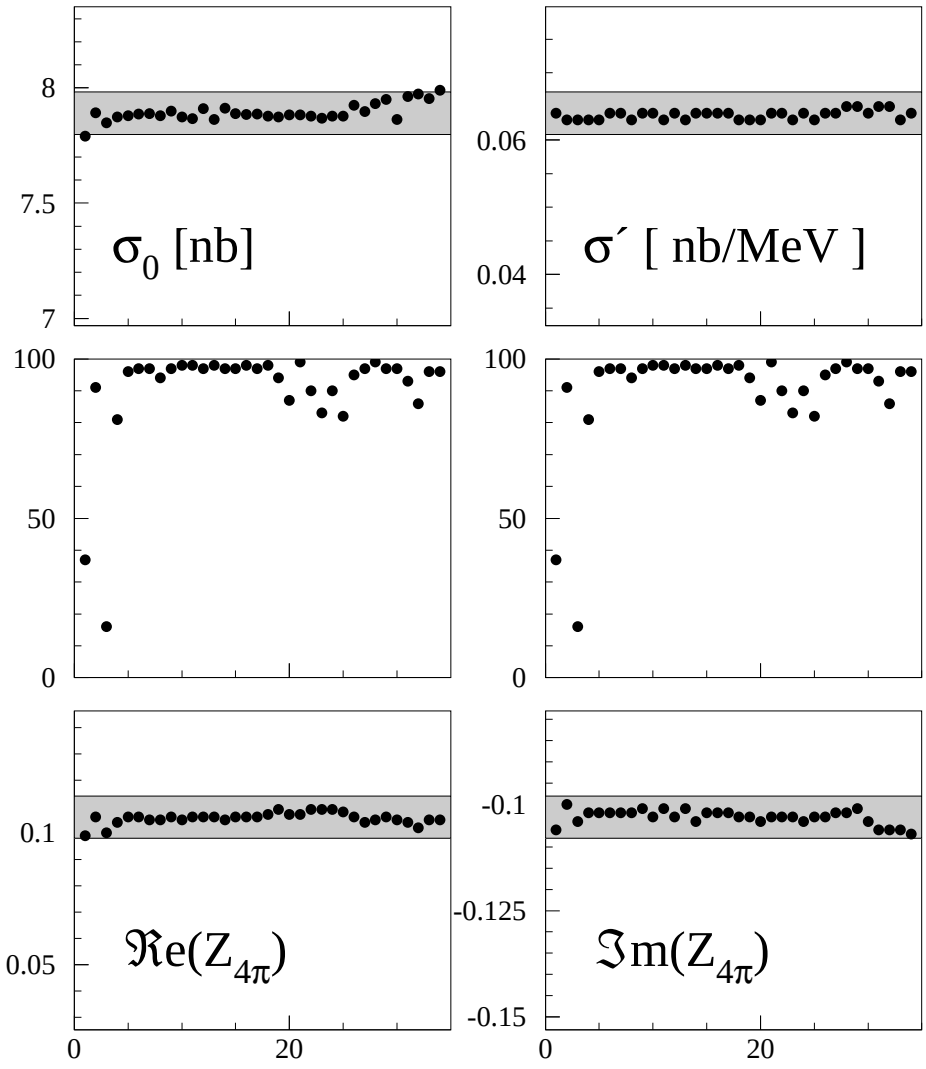

Fig. 30. Complete set of variations of the cross section fit results. Top-left σ_0, top-right: σ', bottom-left: $\Re e(Z)$, bottom-right: $\Im m(Z)$. In the center plots, the value of χ^2 probability of the fit is shown. The gray band represents the full error on the cross section parameters (stat $\oplus$ syst).

11 Fit results and ω branching ratios extraction

Using the present results on the cross section parameters together with the corresponding value obtained for the neutral final state ($\pi^0\pi^0\gamma$ [20]) reported in the Tab. 8, it is possible to extract the value of the dominant BR of the ω meson.

Table 8
Fit results for the $e^+e^- \to \pi^+\pi^-\pi^0\pi^0$ cross section (central column) and for $e^+e^- \to \pi^0\pi^0\gamma$ cross section (right column).

Parameter	$e^+e^- \to \pi^+\pi^-\pi^0\pi^0$	$e^+e^- \to \pi^0\pi^0\gamma$
σ_0 (nb)	$7.89 \pm 0.06 \pm 0.07$	$0.724 \pm 0.010 \pm 0.003$
$\Re e(Z)$	$0.106 \pm 0.007 \pm 0.004$	$0.011 \pm 0.015 \pm 0.006$
$\Im m(Z)$	$-0.103 \pm 0.004 \pm 0.003$	$-0.154 \pm 0.007 \pm 0.004$
σ' (nb/MeV)	$0.064 \pm 0.003 \pm 0.001$	$0.0053 \pm 0.0005 \pm 0.0002$

Removing the common systematics on the luminosity (0.5%), which cancels out in the ratio, from the two KLOE measurements we obtain:

$$\frac{\sigma_0(\omega \to \pi^0\gamma)}{\sigma_0(\omega \to \pi^+\pi^-\pi^0)} = 0.0918 \pm 0.0016 \tag{5}$$

Taking into account the phase space difference between the two decays [18], the ratio of the partial widths can be extracted:

$$\frac{\Gamma(\omega \to \pi^0\gamma)}{\Gamma(\omega \to \pi^+\pi^-\pi^0)} = 0.0897 \pm 0.0016 \tag{6}$$

Since these two final states correspond to the 98% of the ω decay channels, we use the $\Gamma(\omega \to \pi^0\gamma)/\Gamma(\omega \to \pi^+\pi^-\pi^0)$ ratio and the sum of averages of the existing BR measurements on rarest decays [21] to extract the main ω branching fractions, imposing the unitarity relation:

$$BR(\omega \to \pi^+\pi^-\pi^0) = (90.24 \pm 0.19)\% \tag{7}$$
$$BR(\omega \to \pi^0\gamma) = (\ 8.09 \pm 0.14)\% \tag{8}$$

with a correlation of -71%. Comparison between our evaluation and the values in PDG [21] is shown in Fig. 31.

We expect that the parameters describing the non-resonant part of the cross section for the two final states differ for the ratio of the width times a small correction due to different integration on the accessible phase space. In the

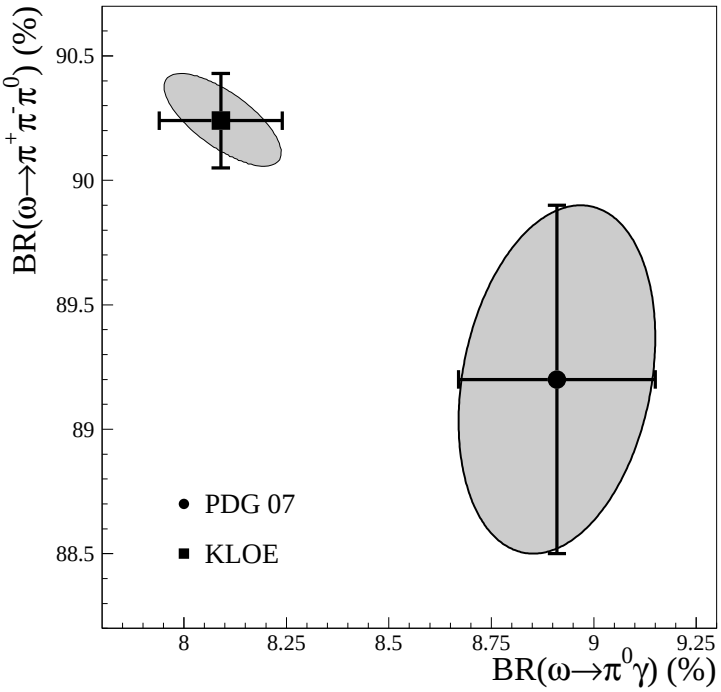

Fig. 31. Branching fraction for the two main ω decay channels. The black square is the KLOE fit result, while the black dot is the PDG constrained fit result. The shaded regions are the 68% C.L.

absence of a detailed calculation of this correction, we have tried a combined fit of the two cross sections including the ratio between them as free parameter. The results are completely in agreement with respect to the two separate fits. The combined fit results shown here in Tab. 9.

Table 9
Fit results for the combined cross section fit. The last two $\pi\pi\gamma$ parameters are calculated from the fit results.

Parameter ($e^+e^- \to \omega\pi^0$)	
$\sigma_0^{4\pi}$ (nb)	7.86 ± 0.05
$\Re(Z_{4\pi})$	0.108 ± 0.006
$\Im(Z_{4\pi})$	-0.102 ± 0.004
$\sigma'_{4\pi}$ (nb/MeV)	0.062 ± 0.003
$\Re(Z_{\pi\pi\gamma})$	0.005 ± 0.013
$\Im(Z_{\pi\pi\gamma})$	-0.157 ± 0.005
Ratio	0.0933 ± 0.0008
$\sigma_0^{\pi\pi\gamma}$ (nb)	0.733
$\sigma'_{\pi\pi\gamma}$ (nb/MeV)	0.0058

12 BR($\phi \to \omega\pi^0$) evaluation

The measured $\sigma_0^{4\pi}$ and $Z_{4\pi}$ parameters of the $\pi^+\pi^-\pi^0\pi^0$ final state are related to the BR($\phi \to \omega\pi^0$) through the relation:

$$BR(\phi \to \omega\pi^0) = \frac{\sigma_0(m_\phi)|Z_{4\pi}|^2}{\sigma_\phi}, \tag{9}$$

where $\sigma_0(m_\phi)$ is the total cross section of the $e^+e^- \to \omega\pi^0$ process and σ_ϕ is the peak value of the production cross section for the ϕ resonance.

Taking the constant terms obtained from the $\pi^+\pi^-\pi^0\pi^0$ corrected with the $BR(\omega \to \pi^+\pi^-\pi^0)$ and the Γ_{ee} measurement from KLOE [22] for the evaluation of σ_ϕ, we extract:

$$BR(\phi \to \omega\pi^0) = (4.4 \pm 0.6) \times 10^{-5} \tag{10}$$

in agreement with the previous measurement from the SND experiment [18].

13 Conclusions

With this work, we have obtained a precise measurement of the cross section parameters for the process $e^+e^- \to \omega\pi^0 \to \pi^+\pi^-\pi^0\pi^0$in the $\sqrt{s}$ range from 1000 to 1030 MeV. Here the interference between the process under study and the resonant process $\phi \to \omega\pi^0$ has been observed and the relative amplitude has been measured. Our results are in good agreement with respect to the previous SND determinantion, significantly improving the accuracy on each parameter. Using this result, together with the correspopnding measurements for the process $e^+e^- \to \omega\pi^0 \to \pi^0\pi^0\gamma$, we have extracted the ratio of ω decay widths: $\Gamma(\omega \to \pi^0\gamma)/\Gamma(\omega \to \pi^+\pi^-\pi^0) = 0.0897 \pm 0.0016$
Combining the latter with the measurements of the rarest decays we have obtained the most precise values for the dominant ω branching fractions: $BR(\omega \to \pi^+\pi^-\pi^0) = (90.24 \pm 0.19)\%$ and $BR(\omega \to \pi^0\gamma) = (8.09 \pm 0.14)\%$. The latter deviates by three standard deviations from the Particle Data Group evaluation as shown in Fig. 31.
Moreover, using our determination of the BR($\omega \to \pi^-\pi^+\pi^0$), together with the cross section parameters for the $\pi^+\pi^-\pi^0\pi^0$ final state we have derived the branching fraction for the OZI and G-parity suppressed decay $\phi \to \omega\pi^0$: $BR(\phi \to \omega\pi^0) = (4.4 \pm 0.6) \times 10^{-5}$.
A comparison between our results and the previous is shown in Fig. 32

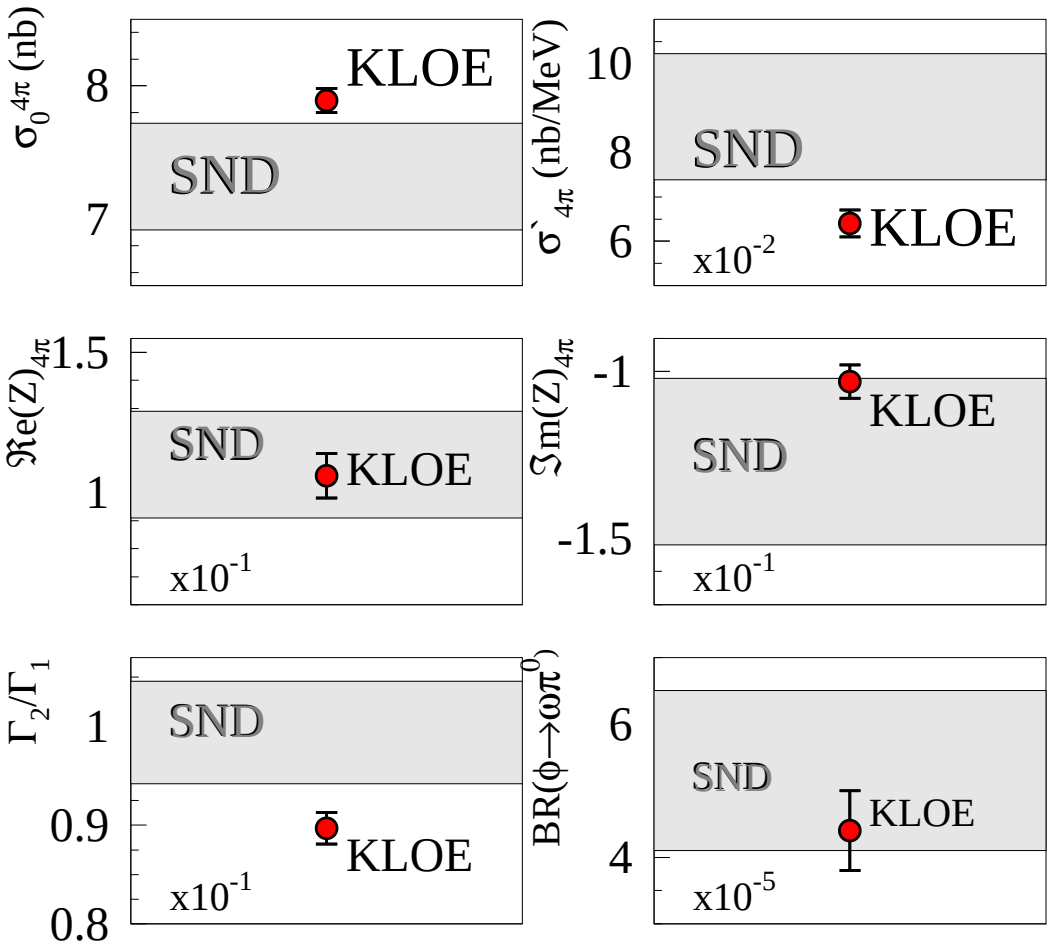

Fig. 32. Comparison between KLOE results and previous measurements. The gray bands stands for the 68% C.L. of the previous measurements, while red dots are the KLOE results.

A Generator

A.1 Process description

In the official release of `GEANFI` (build # 173) the process $\pi^+\pi^-\pi^0\pi^0$ was simulated as a decay chain of two and tree body. For the tree body decay a flat distibution in phase space was assumed. This parametrization is unsuitable for this decay.

The process $\pi^+\pi^-\pi^0\pi^0$ could be described using Vector Meson Dominance (VMD) model, as in [2]. The amplitude for this process is obtained summing the six diagrams summarized in fig. A.1. The general idea of this model is to calculate, for a given four-momenta configuration of four final state pions, the VMD matrix element.

In fig. A.1, neither the ρ meson charge nor the pion four-momenta is specified. The total amplitude is the sum over all permutations $(\rho^0\pi^0) \leftrightarrow (\rho^\pm\pi^\mp)$ and $\pi^0(p_\alpha) \leftrightarrow \pi^0(p_\beta)$.

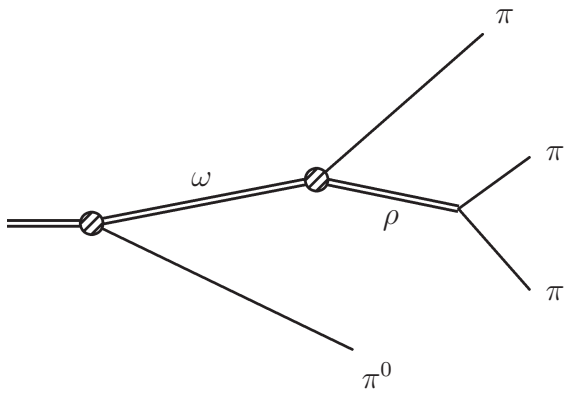

Fig. A.1. VMD diagram fow $\pi^+\pi^-\pi^0\pi^0$.

The corrisponding matrix element is:

$$|\mathcal{M}|^2 = \left|\overrightarrow{J}^{+-00}_{\omega\pi^0}\right|^2 \tag{A.1}$$

where:

$$\overrightarrow{J}^{+-00}_{\omega\pi^0} = G_\omega\left[\overrightarrow{t}_\omega(p_2,p_4,p_1,p_3) - \overrightarrow{t}_\omega(p_2,p_1,p_4,p_3) - \overrightarrow{t}_\omega(p_2,p_3,p_1,p_4)\right] + \tag{A.2}$$

$$G_\omega\left[\overrightarrow{t}_\omega(p_3,p_4,p_1,p_2) - \overrightarrow{t}_\omega(p_3,p_1,p_4,p_2) - \overrightarrow{t}_\omega(p_3,p_2,p_1,p_4)\right]$$

p_j is the four-momentum of pion. The four-momenta are associate to the pions charge as:

$$\pi^+(p_1)\pi^0(p_2)\pi^0(p_3)\pi^-(p_4)$$

In eq. A.2, each term $\overrightarrow{t}_\omega$ is relative to a ρ charge. The difference between the first and second lines is due to π^0 permutation.

Here is the explicit espression of $\overrightarrow{t}_\omega$:

$$\begin{aligned}\overrightarrow{t}_\omega(p_\alpha,p_\beta,p_\gamma,p_\delta) = \frac{F_\omega^2(P-p_\alpha)}{D_\omega(P-p_\alpha)D_\rho(p_\beta+p_\delta)}\Big\{\Big(E_\delta\,\overrightarrow{p}_\gamma - E_\gamma\,\overrightarrow{p}_\delta\Big)\,(\overrightarrow{p}_\alpha\cdot\overrightarrow{p}_\beta) \\ -\overrightarrow{p}_\beta\Big(E_\delta\,\overrightarrow{p}_\alpha\cdot\overrightarrow{p}_\gamma - E_\gamma\,\overrightarrow{p}_\alpha\cdot\overrightarrow{p}_\delta\Big) - E_\beta\Big[\overrightarrow{p}_\gamma\,(\overrightarrow{p}_\alpha\cdot\overrightarrow{p}_\delta) - \overrightarrow{p}_\delta\Big(\overrightarrow{p}_\alpha\cdot\overrightarrow{p}_\gamma\Big)\Big]\Big\}\end{aligned} \tag{A.3}$$

where E_j is the pions energy,

$$D_V(q) = q^2 - M_V^2 + iM_V\Gamma_V\frac{g(q^2)}{g(M_V^2)}$$

is the inverse of V meson propagator,

$$g(s) = s^{-1/2}(s-(\sum_f m_f)^2)^{3/2}$$

is the energy dependence of the width and

$$F_\omega(Q^2) = \frac{1+M_\omega^2/\Lambda^2}{1+Q^2/\Lambda^2}$$

is the form factor for the coupling $\omega\to\rho\pi$.

In the generator we set $g_\omega(s)=1$ and $\Lambda = 1\ GeV$.

A.2 Code structure and performances

Sampling of the probability distribution is made by a simple hit-or-miss procedure. For this reason, the generator has the total energy in input, and the pions' four-momenta and the normalized [10] weight as output.

The central generator routine `WP_PMOO` (see fig. A.2) needs two supplementary routines:

[10] When weight is normalized with is greatest value.

- `RAMBOS:` routine for n-body decay ($n \in [2, 100]$) with uniform distribution in phase space [23];
- `CURRENTTERM:` diagram calculation according to eq. A.3.

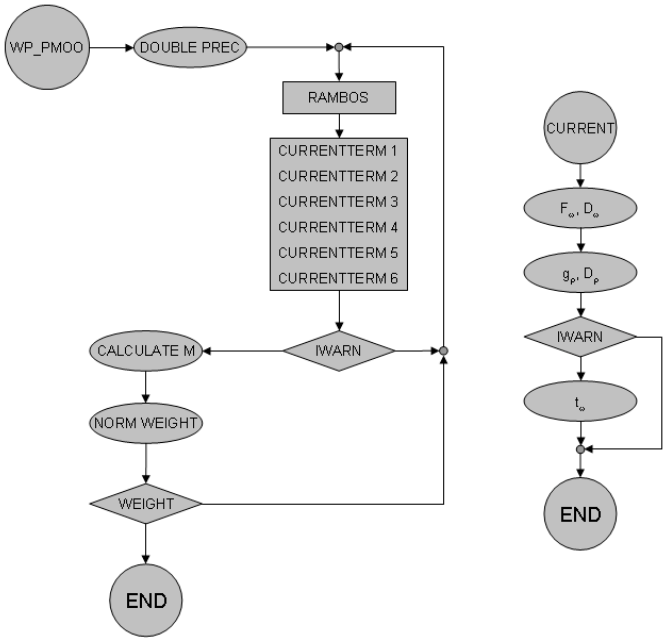

Fig. A.2. Flux diagram of `WP_PMOO`

When all diagrams are correctly calculated and packed in the matrix element, the `WP_PMOO` routine calculates the normalized weight as:

$$WT_{norm} = \frac{|\mathcal{M}|^2 \cdot \Delta\Phi(p_\alpha, p_\beta, p_\delta, p_\gamma)}{WT_{MaX}}$$

WT_{MaX} has been chosen to optimize execution time with respect to the distribution sampling.

A.3 `GEANFI`: change log

The process $\pi^+\pi^-\pi^0\pi^0$ was generated through a call to the routine `OMEPI`, following the flow chart shown in fig. A.3-a. After a complete restyle of the involved routines (`OMEPI` and `OMGDEC`), now the scheme appears as shown in fig. A.3-b.

Source code and reference documentation (in Italian) are available in:

/afs/lnf.infn.it/user/a/adesanti/public/omegapi/mc_src

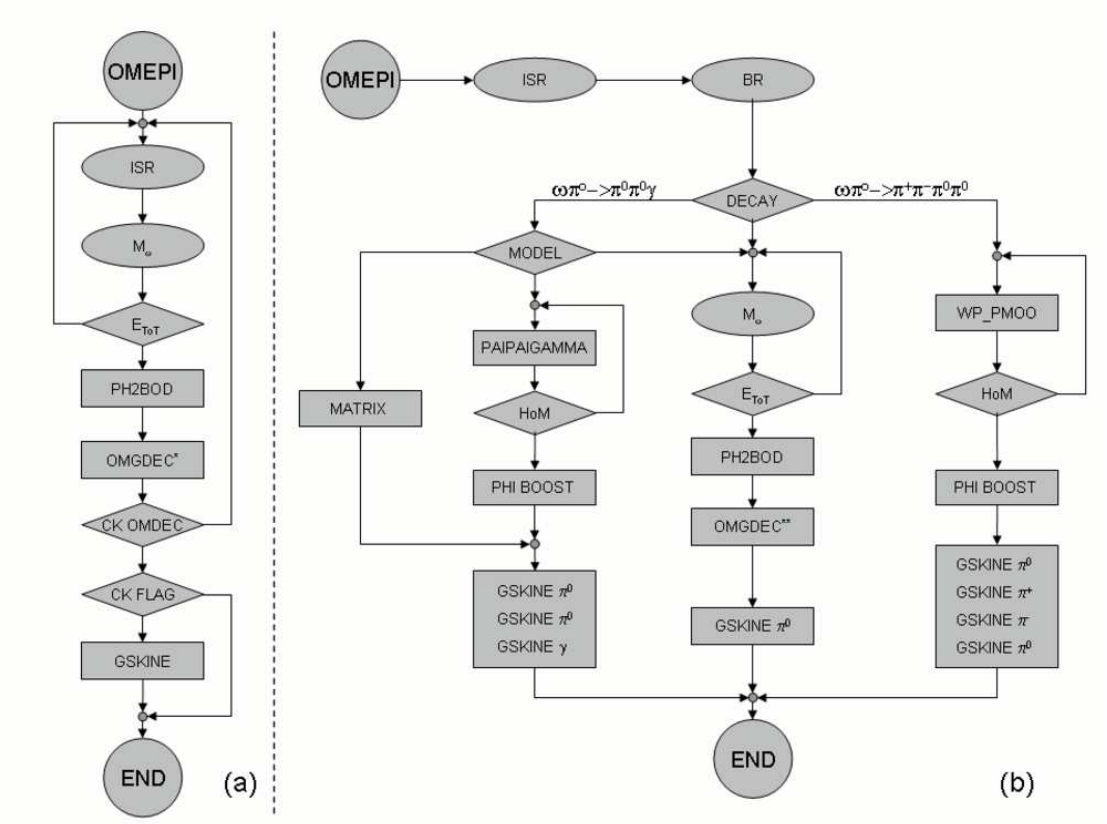

Fig. A.3. Old (a) and new (b) flux diagram for the routine `OMEPI` routine.

References

[1] Achasov, N.N. Kozhevnikov, A.A. . **Decay of ϕ-meson suppressed by OZI and G-Parity. Role of mixing and of direct transition**. *Int.J.Mod.Phys*, 1992.

[2] Akhmetsin, R.R. *et al*. **a1(1260) π dominance in the process $e^+e^- \to 4\pi$**. *Budker INP 98-83 (hep-ex/9904024 v2)*, 1998.

[3] Ambrosino, F. *et al*. **Data handling, reconstruction and simulation for the KLOE experiment.** *KLOE NOTE*, 191, 2004.

[4] Fiore, S., Venanzoni, G. **Quality selection for 2005 data**. *KLOE MEMO*, 231, 2006.

[5] C. M. Carloni Calame, G. Montagna, O. Nicrosini, and F. Piccinini. **The BABAYAGA event generator**. *Nucl. Phys. Proc. Suppl.*, 131:48–55, 2004.

[6] G. Balossini, C. M. Carloni Calame, G. Montagna, O. Nicrosini, and F. Piccinini. **Matrix elements and parton shower in the event generator BABAYAGA**. *Nucl. Phys. Proc. Suppl.*, 162:59–62, 2006.

[7] Antonelli, M. and Dreucci, M. **Measurement of the K_0 mass from $\phi \to K_S K_L$, $K_S \to \pi^+\pi^-$**. *KLOE NOTE*, 181, 2002.

[8] R. Stroili. **measurement of the $e^+e^- \to \pi^+\pi^-\pi^+\pi^-$, $K^+K^-\pi^+\pi^-$, $K^+K^-K^+K^-$cross sections using initial state radiation at babar**. *AIP Conf. Proc.*, 717:55–59, 2004.

[9] M. *et al* Greco. **Radiative Bhabha scattering at DAΦHNE**. *Phys. Lett.*, B318:635–641, 1993.

[10] E. A. Kuraev and Victor S. Fadin. **On radiative correction to e^+e^- single photon annihilation at high energy**. *Sov. J. Nucl. Phys.*, 41:466–472, 1985.

[11] Gatti, C., Palutan, M. and Spadaro, T. **Measurement of $\Gamma(K_S \to \pi^+\pi^-(\gamma))/\Gamma(K_S \to \pi^0\pi^0)$ with 2001-2002 data**. *KLOE NOTE*, 209, 2006.

[12] Ambrosino, F. *et al*. **The Event classification procedure**. *KLOE MEMO*, 255, 2000.

[13] De Santis, A., Versaci, R. **Tracking and vertexing efficiencies studies using a rhopi sample for 2002 and 2005 data**. *KLOE MEMO*, 343, 2008.

[14] Antonelli, M., Ingrosso, L., Incagli, M., Miscetti, S. **The Track to Cluster association program**. *KLOE MEMO*, 129, 1996.

[15] CERN. **HBOOK Ref manual V. 4.20**. *CERN Program Library Long Writeup*, Y250:120–126, 1993.

[16] Denig, A., Ngyen, F. **The KLOE Luminosity Measurement**. *KLOE NOTE*, 202, 2005.

[17] E. Barberio and Z. Was. **PHOTOS: A Universal Monte Carlo for QED radiative corrections. Version 2.0**. *Comput. Phys. Commun.*, 79:291–308, 1994.

[18] Aulchenko, V.M. Achasov, M.N. *et al*. **The Process $e^+e^- \to \omega\pi^0$ near the ϕ resonance**. *Journal of Experimental and Theoretical Physics*, Vol 90 No 6, 2000.

[19] **http://www.lnf.infn.it/kloe/private/bes2002.html**.

[20] De Santis, A., Giovannella, S., Miscetti, S. **Study of the process $\pi^0\pi^0\gamma$with 2001/2002 KLOE data**. *KLOE MEMO*, 344, 2008.

[21] Yao, W. -M. *et al*. **Review of particle physics: 2007 partial update for 2008 edition**. *http://pdg.web.cern.ch/pdg*, 2008.

[22] F. *et al* Ambrosino. **Measurement of the leptonic decay widths of the Phi-meson with the KLOE detector**. *Phys. Lett.*, B608:199–205, 2005.

[23] Kleiss, R., Stirling, W. James, Ellis, S. D. **A new Monte Carlo treatment of multiparticle phase space at high-energies**. *Comput. Phys. Commun.*, 40:359, 1986.

KLOE NOTE are public in the documents section of the KLOE experiment website:
http://www.lnf.infn.it/kloe/